

Perspective

Computational Design of Thermally Activated Delayed Fluorescence Materials: The Challenges Ahead

Yoann Olivier, Juan Carlos Sancho-García, Luca Muccioli, Gabriele D'Avino, and David Beljonne

J. Phys. Chem. Lett., **Just Accepted Manuscript** • DOI: 10.1021/acs.jpcllett.8b02327 • Publication Date (Web): 28 Sep 2018

Downloaded from <http://pubs.acs.org> on September 29, 2018

Just Accepted

“Just Accepted” manuscripts have been peer-reviewed and accepted for publication. They are posted online prior to technical editing, formatting for publication and author proofing. The American Chemical Society provides “Just Accepted” as a service to the research community to expedite the dissemination of scientific material as soon as possible after acceptance. “Just Accepted” manuscripts appear in full in PDF format accompanied by an HTML abstract. “Just Accepted” manuscripts have been fully peer reviewed, but should not be considered the official version of record. They are citable by the Digital Object Identifier (DOI®). “Just Accepted” is an optional service offered to authors. Therefore, the “Just Accepted” Web site may not include all articles that will be published in the journal. After a manuscript is technically edited and formatted, it will be removed from the “Just Accepted” Web site and published as an ASAP article. Note that technical editing may introduce minor changes to the manuscript text and/or graphics which could affect content, and all legal disclaimers and ethical guidelines that apply to the journal pertain. ACS cannot be held responsible for errors or consequences arising from the use of information contained in these “Just Accepted” manuscripts.



Computational Design of Thermally Activated Delayed Fluorescence Materials: The Challenges Ahead

Y. Olivier,¹ J.-C. Sancho-Garcia,² L. Muccioli,³ G. D'Avino,⁴ D. Beljonne¹

¹Laboratory for Chemistry of Novel Materials, University of Mons, Place du Parc 20, B-7000 Mons, Belgium.

²Departamento de Química Física, Universidad de Alicante, E-03080 Alicante, Spain.

³Dipartimento di Chimica Industriale "Toso Montanari", Università di Bologna, I-40136 Bologna, Italy, and Institut des Sciences Moléculaires, UMR 5255, University of Bordeaux, F- 33405 Talence, France.

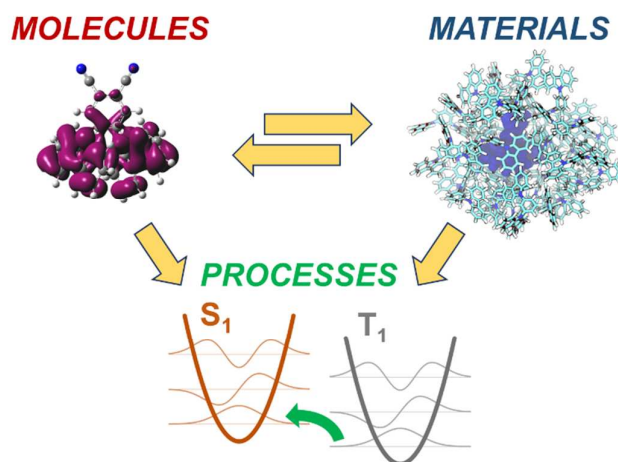
⁴Institut Néel, CNRS and Grenoble Alpes University, F-38042 Grenoble, France.

Corresponding author: David.beljonne@umons.ac.be

Abstract

Thermally activated delayed fluorescence (TADF) offers the premise for all-organic light emitting diodes with quantum efficiencies competing those of transition metal-based phosphorescent devices. While computational efforts have so far largely focused on gas-phase calculations of singlet and triplet excitation energies, the design of TADF materials requires multiple methodological developments targeting among others a quantitative description of electronic excitation energetics, fully accounting for environmental electrostatics and molecular conformational effects, the accurate assessment of the quantum-mechanical interactions that trigger the elementary electronic processes involved in TADF, as well as a robust picture for the dynamics of these fundamental processes. In this perspective, we describe some recent progress along those lines and highlight the main challenges ahead for modeling, which we hope will be useful to the whole TADF community.

TOC Figure: Multiscale TADF molecular-based design



Organic light-emitting diodes (OLEDs) have emerged as a mature technology, reaching commercial applications in lighting and full-color displays. Delayed emission with characteristic spectra coinciding with prompt fluorescence but differing in the emission lifetimes has been observed in eosin solutions and has since been known as E-type fluorescence¹. This is also referred to as Thermally Activated Delayed Fluorescence (TADF), a process that offers the premise to boost internal quantum efficiency (IQE) of electroluminescence beyond the 25% spin statistical limit. The demonstration of TADF in OLEDs has shifted the material design paradigm from phosphors containing rare and expensive transition metals towards all-organic compounds with reduced singlet-triplet exchange interactions.

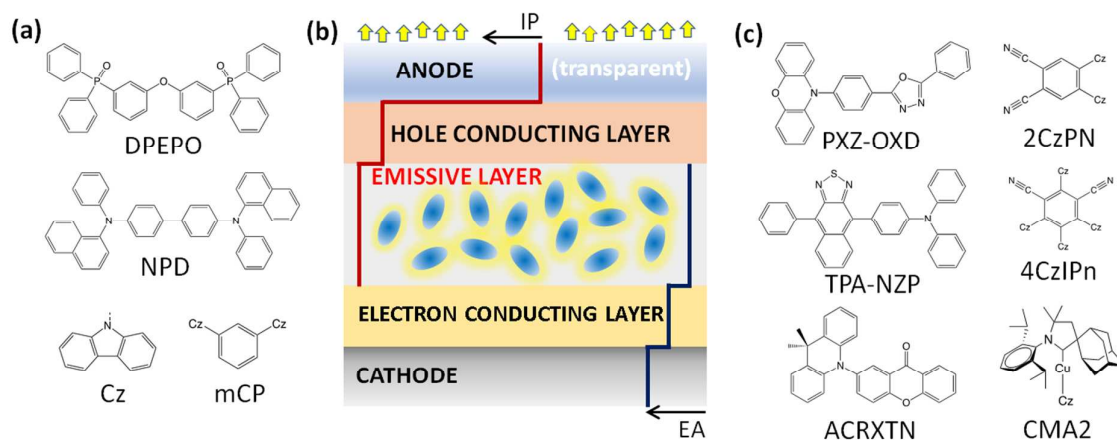


Figure 1: (a) Chemical structures of some relevant host materials: Bis[2-(diphenylphosphino)phenyl] ether oxide (DPEPO), N,N'-Bis(naphthalen-1-yl)-N,N'-bis(phenyl)benzidine, (NPd) and 1,3-Di(9H-carbazol-9-yl)benzene, 9,9'-(1,3-Phenylene)bis-9H-carbazole (mCP). Chemical structure of the carbazole (Cz) group. (b) Minimal sketch of a TADF-doped OLED, where electron and hole conducting layers serve also as hole and blocking layers, respectively, and as exciton blocking layer. Dark blue and red lines indicate typical levels for electron affinities and ionization potentials. This perspective focuses only on the emissive layer, where electron and holes recombine to form an exciton. The layer is constituted of a hole and electron conducting matrix (host), containing a few percent of TADF emitters (guest). The ideal host should possess EA (IP) values lower (higher) than the emitter. (c) Chemical structures of emitters discussed in the text: phenoxazine-2,5-diphenyl-1,3,4-oxadiazole (PXZ-OXD), 4,5-di(9H-carbazol-9-yl)phthalonitrile (2CzPN), N,N-diphenyl-4-(9-phenylnaphtho-[2,3-c][1,2,5]-thiadiazol-4-yl)aniline (TPA-NZP), 2,4,5,6-Tetra(9H-carbazol-9-yl)isophthalonitrile (4CzIPn), 3-(9,9-dimethylacridin-10(9H)-yl)-9H-xanthen-9-one (ACRXTN) and Cyclic (alkyl)(amino)carbene ligands copper-carbazole (CMA2).

1
2
3 TADF emission is triggered by Reverse InterSystem Crossing (RISC) from the non-radiative triplet
4 'reservoir' states to radiative singlet states², a process that is facilitated by a small energy splitting
5 ΔE_{ST} between the lowest singlet (S_1) and triplet (T_1) excited states, and possibly assisted by the
6 manifold of higher-lying triplet states (T_n , see Figure 2)³⁻⁵. Hence, both prompt (from the lowest
7 singlet) and delayed (from upconverted triplets) fluorescence decay channels add up in converting
8 into light potentially all electrically generated excitons, irrespective of spin. The most common design
9 strategy of TADF emitters consists in partitioning hole and electron densities over different spatial
10 regions via electron donating (D) and accepting (A) units, often connected in a twisted conformation,
11 hence reducing exchange interactions splitting singlets from triplets⁶⁻⁹. In actual cases, the excited
12 states involved in TADF often turn out to be hybrid mixtures of charge transfer (CT) and local
13 excitation (LE) diabatic states, with the amount of mixing prompted by vibronic coupling^{10,11}. We
14 refer the interested reader to a recently published review¹² for a critical discussion of the chemical
15 design rules that have emerged so far through the fruitful interplay between theoretical and
16 experimental chemists. Despite some progress has been achieved, molecular design has largely relied
17 on the calculation of excitation energies from the optimized ground-state geometry using time-
18 dependent density functional theory (TD-DFT), either for isolated molecules or assuming a
19 continuum embedding (as for instance described using polarizable continuum models, PCM)¹³⁻¹⁵. The
20 sole criterion for the selection of potential candidates for TADF is then the calculated exchange gap,
21 ΔE_{ST} , vertical or adiabatically, between the lowest singlet and triplet excitations. Besides raising a
22 number of important technical questions regarding the accuracy of the predictions, this simplified
23 view of the TADF mechanism might considerably bias the engineering rules, as it neglects potentially
24 important effects such as the specifics of intramolecular conformation and intermolecular (host-
25 guest) interactions on spin conversion dynamics in the solid state. This perspective aims at bringing a
26 comprehensive view on the modeling of TADF emitters and at highlighting the challenges ahead. For
27 being predictive, we argue that TADF-oriented computational models should include in an integrated
28 framework¹⁰:

- 29 1) An accurate description of the singlet and triplet excited-state manifolds in terms of their
30 relative energy and detailed nature, including coupling to relevant vibrational degrees of
31 freedom;
- 32 2) A reliable evaluation of spin-orbit and hyperfine couplings mediating (reverse) singlet-triplet
33 intersystem crossing;
- 34 3) A proper embedding scheme to account for both structural and electrostatic effects in the
35 emitting layer;

4) A solver for excited-state dynamics that includes electron-phonon and spin-mixing interactions on an equal footing.

In the following, the needed methodologies to reach these ambitious targets are critically reviewed and discussed, going all the way from a quantum-chemical description of the molecular TADF building blocks to the simulation of the corresponding solid-state materials using combined quantum-classical methods.

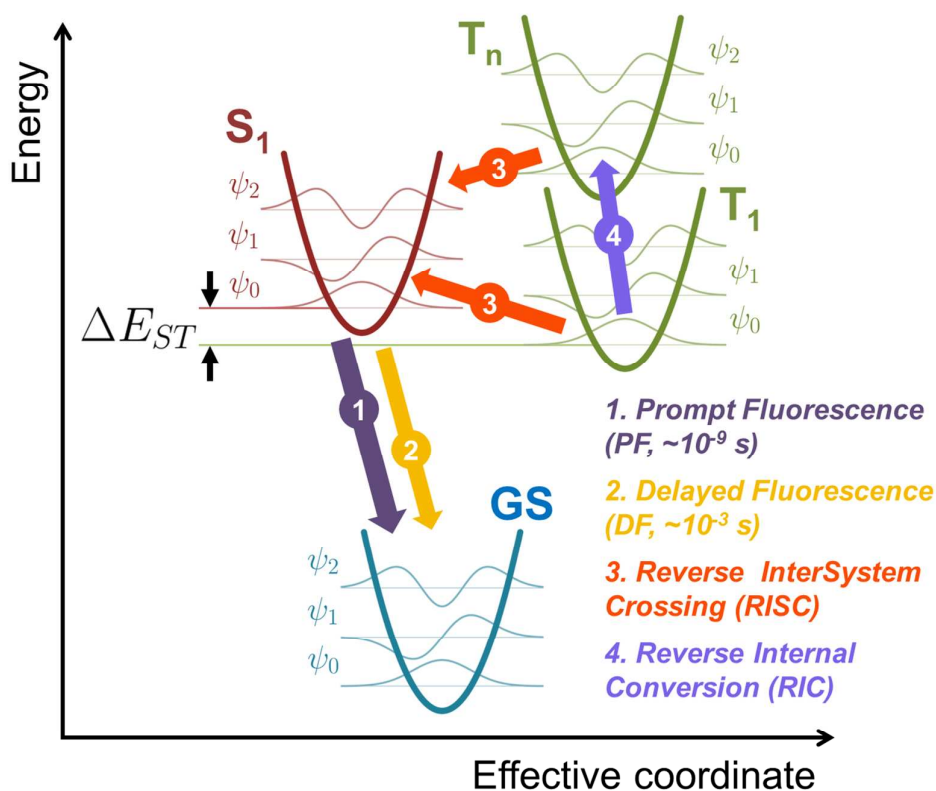


Figure 2 : Illustration of the electronic states involved in TADF, i.e. ground (GS), singlet (S_0) and triplet (T_0 , T_n) excited states along an effective vibrational coordinate. The elementary steps leading to prompt (PF) and delayed (DF) fluorescence are illustrated as arrows. Low-quanta vibrational wavefunctions, which promote reverse intersystem crossing (RISC) and reverse internal conversion (RIC), are also shown.

1
2
3 Generally speaking, the set of molecules acting as hosts or emitters share a common feature, that is,
4 a relatively large size compared to those molecules constituting the datasets used for historically
5 benchmarking *ab initio* methods^{16–18}. We focus here on modern variants of *ab initio* theories for
6 excited states, particularly for calculating vertical transition energies to the lowest excited-state of
7 singlet and triplet spin symmetry, $\Omega(S_1)$ and $\Omega(T_1)$ respectively, also applicable to the whole manifold
8 of S_n and T_n states. Although in principle superior to all other amenable approaches, due to the
9 unfavorable scaling with system size (N) of the family of methods based on iterative coupled-cluster
10 (CC) equations (Ω), their application to TADF compounds have been severely limited and only recently
11 some examples applying the hierarchy of CC-based methods to small molecules have appeared¹⁹.
12 Actually, for CC-based methods, the hierarchy is CC2 (N^5) < CCSD (N^6) < CC3 (N^7) < CCSDT (N^8),
13 concerning both computational scaling with system size (N) and expected accuracy. Note also that
14 CC2 (CC3) is an approximation to CCSD (CCSDT) that has been developed with the prediction of
15 excited-state energies as the main focus, and that all these variants are based on linear-response
16 theory. On the other hand, EOM-CCSD (N^6) is based on a slightly different theoretical frame, though
17 it leads to similar excitation energies (yet different transition dipole moments).
18
19

20
21
22
23
24
25
26
27 The accuracy of the methods is very high, e.g. CCSDT excitation energies are within a few tens of meV
28 w.r.t. FCI, but they are only amenable to very small molecules, hence not applicable for most TADF
29 chromophores. Yet, simplified versions of second-order wavefunction methods, and thus with a
30 reduced formal scaling of $O(N^5)$ with respect to both canonical equations and higher-order methods
31 such as CCSDT, are available. We mention, among them, linear-response CC2 and ADC(2) as emerging
32 cost-effective and accurate methods²⁰. Note that in the case of CC2, due to the fact that the full
33 expression for double amplitudes is retained only at first-order, the method behaves better for single
34 excitations and tends to overestimate excitations energies for doubly excited states. The ADC(2)
35 method suffers from the same inherent limitation for double excitations, and the corresponding
36 ADC(3) is too costly for routine calculations, although it leads to reliable benchmarks. However, the
37 extended ADC(2)-x version provides an overall improvement for the description of excited states with
38 double-excitation character. An interesting compromise between accuracy and computational cost is
39 provided by the spin-component-scaling (SCS-)CC2 method, through the introduction of scaling
40 factors to the same-spin and opposite-spin contributions of the second-order correlation energy,
41 leading thereby a better performance for excited states²¹. There are other methods that allow, by
42 construction, n - or multi-electron excitations, that is by promoting up to n electrons into an active
43 window of m molecular orbitals, as in RAS- or CASSCF/CASPT2 methods. However, computational
44 limitations preclude the use of large (n,m) active spaces ideally including all relevant π and π^*
45 orbitals. We finally mention many-body Green's function methods such as the *GW* plus Bethe-
46
47
48
49
50
51
52
53
54
55
56
57
58
59
60

1
2
3 Salpeter equation (BSE) formalisms, also explored recently within this context with some success^{22,23}.
4 We shall, however, remark that full BSE suffers the issue of triplet instability, much as TD-DFT does²⁴
5 (see below).
6
7

8 As other possible caveats for these calculations, we here mention: (i) the very costly calculation of
9 excited-state geometries and adiabatic values for $\Omega(S_1)$ and $\Omega(T_1)$, which are important figures when
10 dealing with light emission; and (ii) the marked dependence (i.e. slow convergence) with basis sets
11 size expected for these methods and the possible need to include diffuse functions. This has
12 historically prompted the use of more cost-effective methods, despite the fact that the
13 computational efforts needed for *ab initio* calculations can be reduced by using resolution-of-the-
14 identity^{25,26}, or density-fitting techniques²⁷. To conclude, so far, wavefunction-based methods are not
15 routinely used for TADF applications and TD-DFT is usually preferred. However, they offer a robust
16 framework to tackle challenging issues, such as assessing the contribution to RISC of higher-lying
17 singlet and triplet excited states²⁶ or modeling multiple resonance effects^{28,29}.
18
19
20
21
22
23

24 Due to the need to handle large molecular sizes and to achieve a good trade-off between accuracy,
25 scaling, and feasibility of the calculations for the fast screening of compounds, (Time-Dependent)
26 Density Functional Theory, (TD-)DFT methods are by far the most employed computational tools in
27 the TADF community. However, contrarily to what was initially thought, the reliability of the results
28 depends not only on the functional choice for the time-dependent part, but also on the whole
29 computational protocol employed including geometrical and basis sets issues, as well as on the
30 chemical nature of the target molecule. We focus next on excited-state properties of emitters, for
31 which a relatively wide body of information is available from the recent literature.
32
33
34
35
36
37

38 Earlier calculations combined the use of the B3LYP functional with a moderate basis set such as 6-
39 31G* to obtain ground-state geometries and dissect the spatial shape and energy location of the
40 frontier molecular orbitals^{30,31}. When applied to the calculation of vertical transition energies to the
41 lowest excited state of singlet and triplet spin symmetry and their difference dubbed as ΔE_{ST}^V , the
42 results were found to critically depend on the weight, or proportion, of the exact-like exchange
43 introduced into the hybrid functional (typically ranging from 5 to 40%, namely 20% for the widely
44 used B3LYP model)³². Note that any general protocol should give accurate excitation energies for the
45 lowest singlet and triplet excited states, without relying on any error cancellation and without
46 limiting the focus to the magnitude of ΔE_{ST}^V as unique target. Namely, a system- and state-dependent
47 procedure should be avoided, as extension to excited states beyond S_1 and T_1 might be problematic.
48 Since organic molecules are known to benefit from higher-than-defaults (e.g. default values for
49
50
51
52
53
54
55
56
57
58
59
60

1
2
3 B3LYP and PBE0 are 20% and 25% respectively) weights of the exact-like exchange, other functionals
4 like M06-2X have also been used with some success up to now³³.
5

6
7 A major breakthrough was found after imposing the Tamm-Dancoff approximation (TDA) for the
8 solution of the full TD-DFT equation³⁴, which improves the accuracy of routine calculations. This is
9 especially true for T_1 states where TDA cures for the triplet instability problem and, as a result, yields
10 improved ΔE_{ST}^V values. Note that the Thomas-Reiche-Kuhn sum rule for oscillator strengths (i.e. the
11 sum of all oscillator strengths from a particular state to all other equals the number of electrons in
12 the system) is no longer fulfilled with TDA-DFT, as it happened with CIS too. That violation can lead to
13 inaccurate oscillator strength distribution, and thus precludes a state-by-state quantitative
14 comparison of oscillator strength values between theories fulfilling (i.e. TD-HF and TD-DFT) or
15 violating the rule. The PBE0 functional was also applied with some correction for dispersion, i.e.
16 D3(BJ), intended mostly to provide more accurate ground- and excited-state geometries after
17 including non-covalent (intramolecular) effects, and used with large basis sets, i.e. def2-TZVP, to
18 estimate $\Omega(S_1)$ and $\Omega(T_1)$ energies at the (nearly) complete basis set limit. However, while accuracy
19 reaching 0.1-0.2 eV can be achieved for ΔE_{ST}^V values¹³, studies using this computational protocol have
20 not yet been extended beyond S_1 and T_1 states, and thus further efforts are still needed in this
21 direction.
22
23
24
25
26
27
28
29
30

31 Another strategy is provided by range-separated hybrid functionals, i.e. CAM-B3LYP or ω B97X as
32 paradigmatic examples, in which the range-separation parameter may be fine-tuned for each
33 compound^{14,35}, as well as for isolated or host-embedded emitters. In these range-separation models,
34 the electron-electron interaction is split into two contributions, short- and long-range, treating each
35 one at a different theoretical level (short-range often with a semi-local GGA exchange functional and
36 long-range with exact-like exchange to obtain the desired correct asymptotic behavior). The first
37 mention in literature was due to A. Savin et al. in 1997,³⁶ but for the coupling of multiconfigurational
38 ab initio with DFT methods, with probably the first application to GGA exchange functionals by K.
39 Hirao et al. in 2001,³⁷ and popularized later by N.C. Handy et al. with the CAM-B3LYP method.³⁸ Since
40 the tuning of the ω parameter aims at accurately reproducing one-electron attachment/detachment
41 energies, it also naturally leads to accurate HOMO-LUMO gaps and corresponding excited-state
42 energies (relying heavily on that energy difference, to first order). However, more work is still needed
43 to confirm the accuracy of these methods for higher-lying singlets and triplets.
44
45
46
47
48
49
50

51
52 S_1 and T_1 optimized excited-state geometries are now routinely computed from linear-response
53 TD(A)-DFT. However, different options such as the use of UKS (for T_1) or ROKS (for S_1 and T_1 states)
54 exist³⁹. Still, we stress that mixing different levels of theory such as TD(A)-DFT (for S_1) and UKS (for T_1)
55
56
57
58
59
60

1
2
3 can lead, in some instances, to spurious negative values of ΔE_{ST} ^{14,40}. The fast screening of TADF
4 molecules would also benefit of low-cost TD-DFT based methods, such as e.g. sTDA-DFT or sTDA-
5 xTB⁴¹. It would also be desirable to extend these methods beyond one-electron effects. The use of a
6 (D)-like correction introduced by double-hybrid methods, namely a MP2-like term added non self-
7 consistently to the standard TD-DFT treatment, or the coupling of DFT with MRCI (DFT/MRCI), are
8 among the envisioned possibilities, although the price to pay is a higher formal scaling, $O(N^5)$ in the
9 case of double-hybrid functionals. While double-hybrid models appear robust for $\Omega(S1)$ values, the
10 lack of implementations for the calculation of the corresponding $\Omega(T1)$ values has precluded so far
11 the evaluation of ΔE_{ST}^V ⁴². DFT/MRCI has been recently extended to deal with higher-order
12 excitations in multichromophoric systems⁴³, opening new possibilities for exploring light-emission
13 mechanisms for which both singlet and triplet states are of importance, as well as their possible
14 modulation by environmental effects⁴⁴.

21 The need for quantifying the nature of the excited states involved in the TADF process has led to the
22 development of a set of metrics able namely to gauge the CT versus LE character of the excitations,
23 which is critically entangled with the molecular geometry and its fluctuations around
24 equilibrium^{10,43,45}. The existing metrics can be classified into two groups, those based on molecular
25 orbitals, be them KS or NTO, and those based on density differences. Note that the metrics are
26 intended to be: (i) generally applicable, in the sense that they can be applied to any of the desired
27 singlet or triplet excited states; and (ii) easily transferable, with the results not expected to heavily
28 depend on the functional and/or basis set choice. However, the use of relaxed and unrelaxed density
29 might introduce some difference from a quantitative standpoint⁴⁶ as it was recently disclosed.

36 Table 1 summarizes the observables developed so far and their typical values for the limiting cases of
37 pure CT and LE. As regards the first category of tools, the metrics Λ roughly measures the overlap
38 between a pair of occupied (*i*) and virtual (*a*) orbitals involved in the ground-to-excited state
39 transition^{47,48}; other approaches, such as Δr ^{49,50}, aim at giving an effective hole-electron separation
40 during the excitation. On the other hand, for density-based descriptors, the D_{CT} index is based on the
41 barycenters of densities associated with an electronic transition⁵¹, while Φ_S refers to the overlap
42 between the attachment/detachment densities, that is, the electron density removed/rearranged
43 during the excitation⁵². In some cases, due to a spurious behavior of density functionals for CT states,
44 low-lying but unreal (intruder) CT states can appear, which can be also identified and discarded on
45 the basis of the evaluation of intermolecular electrostatic interactions, e.g. by the M_{AC} metrics⁵³.
46 Despite the appearance of a few topological metrics in the last years, there is also convincing
47 evidence that these are highly correlated, as recently shown for a large sample of molecules
48
49
50
51
52
53
54
55
56
57
58
59
60

displaying CT excitations,⁵⁴ which should facilitate comparison between different existing or future studies.

Table 1. Summary of the metrics most used and their limiting values in the case of pure CT and LE excitations.

Metrics	Description	Distinction between the nature of excited-states	
		CT	LE
Λ_{ia}	Overlap between the <i>ia</i> pair of the norms of molecular orbitals	$\Lambda \sim 0$	$\Lambda \sim 1$
Δr	Coefficient-weighted hole-electron distance between a set of orbital centroids	$\Delta r > 2 \text{ \AA}$	$\Delta r < 2 \text{ \AA}$
D_{CT}	Distance between barycenters of density variations (average between the corresponding barycenters)	$t - D_{CT} > 1.6 \text{ \AA}$	$t - D_{CT} < 1.6 \text{ \AA}$
Φ_s	Normalized overlap between attachment/detachment densities	$\Phi_s \sim 0$	$\Phi_s \sim 1$

Metrics based exclusively on orbitals raise some concern. For instance, many-electron excited states might involve multiple pairs of orbitals, thus casting doubt on the meaning of the Λ value. Another example is the case of a symmetric D-A-D triad, where the hole and electron centroids can spuriously occupy similar spatial positions, hence leading to a vanishing value of Δr , despite a strong CT excited-state character. D_{CT} and Φ_s overcome these limitations and appear as more universal metrics⁵⁵.

Interestingly, the use of these metrics has clearly evidenced that the excited states involved in the TADF process are neither full CT or LE, as abusively claimed when discussing the photophysics of TADF emitters^{3,5}, but most often feature a rather mixed CT-LE character^{7,10,56} (see Figure 3a). The amount of CT-LE mixing is controlled by the magnitude of the D-A electronic coupling, which is in turn governed by structural parameters (such as the torsion angle between the two moieties)^{7,10}. While the S_1 excited state often displays a large CT character (small Φ_s ⁷ and large Δr ¹³, see Figure 3a), especially in conformations with near orthogonal D and A moieties⁶, this is less true for the T_1 excited state. This arises from exchange interactions that stabilize localized triplets more than their singlet counterparts, thereby prompting a more intimate LE-CT mixing in the triplet manifold^{7,57}.

From a practical point of view, the metrics presented in table 1 have been applied as a tool to rationalize the ΔE_{ST} and oscillator strength values in TADF compounds. Especially, it has been evidenced that the nature of T_1 is the limiting factor in order to minimize ΔE_{ST} . The nature of T_1 can

be directly probed experimentally by extracting the Zero-Field Splitting (ZFS) parameters from Electron Spin Resonance (ESR) spectroscopy studies. The dominant dipole-dipole component to the ZFS parameters is indeed inversely proportional to the third power of the interspin distance⁵⁸. The larger the CT character of the triplet excited state, the larger the effective electron-hole radius and spin-spin distance and the lower the ZFS parameter value. From a computational point of view, the ZFS parameter can be evaluated through unrestricted DFT calculations using EPR-II and EP-III basis sets that are optimized for the computation of hyperfine coupling constants⁵⁹. Interestingly, a recent study of carbazolyl-dicyanobenzene based TADF emitters (2CzPN and 4CzIPN) has demonstrated that ZFS (as calculated at the UKS level) and Φ_S (obtained from TDA-DFT) values go in par, offering the possibility to confront experimental and theoretical metrics of the triplet excitations⁶⁰ (see Figure 3b). As for singlet excitations, calculated oscillator strengths have been shown to correlate very well to Δr^{11} and overlap metrics such as Λ_{ia} ⁶¹ and Φ_S ⁷.

Finally, we mention that only some of the metrics above can be calculated with common quantum chemistry codes, while others require post-processing after the TD(A)-DFT run. More automated procedures, and further benchmarking, are definitively needed, as well as their integration in large-scale computational codes.

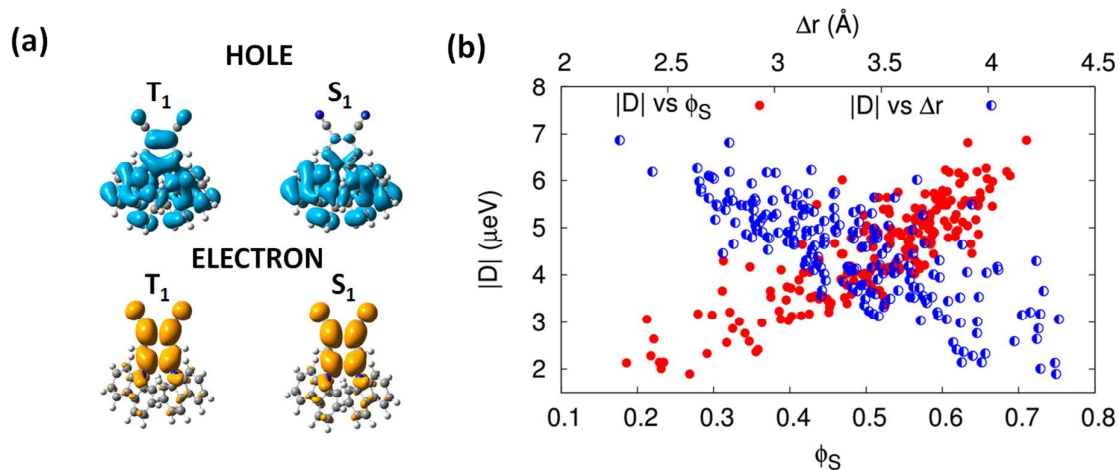


Figure 3: (a) Hole and electron densities calculated in the attachment/detachment formalism for T_1 and S_1 excited states for 2CzPN. (b) Absolute value of the T_1 Zero-Field splitting parameter as a function of the overlap between the hole and electron densities ϕ_S and the distance between the hole and electron densities centroids Δr , as calculated in the attachment/detachment formalism for 2CzPN T_1 excited state. Reprinted and adapted with permission from reference¹⁰. Copyright 2017 by the American Physical Society

Non-radiative processes are playing a key role in determining the internal quantum efficiency of TADF-based devices. On the one hand, reverse intersystem crossing (RISC) and reverse internal

1
2
3 conversion (RIC) are promoting the upconversion from the triplet to the singlet excited-state
4 manifold. On the other hand, ISC favors the generation of triplets that could subsequently be
5 recycled to S_1 or, because of their long lifetime, could decay through triplet-triplet or triplet-polaron
6 annihilation, processes giving rise to device efficiency roll-off at high luminance. Of course, also non-
7 radiative decays to the ground state from both the lowest singlet and triplet states are competing
8 pathways reducing IQE. In the following, we distinguish between spin-conserving, namely (R)IC,
9 triplet-triplet and triplet-polaron annihilation, and spin-non-conserving processes, namely ISC and
10 RISC. Conformational effects on light emission and ISC and RISC are discussed thoroughly below.

11
12 Spin-orbit is a relativistic effect that is responsible for mixing orbital and spin degrees of freedom,
13 thus allowing electronic states of different multiplicities to couple. Spin-orbit coupling naturally arises
14 from the one-electron Dirac equation. Even though being of a fundamental interest, it cannot be
15 solved exactly when considering large many-electron systems such as TADF molecules. Practical
16 applications thus rely on perturbative approaches to non-relativistic electronic structure calculations.
17 Among the most commonly reported approaches, we distinguish the zero-order relativistic
18 approximation (ZORA) from the full Breit-Pauli Hamiltonian (including relativistic mass corrections
19 and spin-orbit effects) and its mean-field approximation that are implemented in a number of
20 softwares based on CASSCF⁶², TD-DFT and DFT-MRCI⁴³ excited-state descriptions. The interest in spin-
21 orbit coupling calculations in the field of OLEDs dates back from the emergence of phosphorescent
22 emitters containing heavy metal centers allowing for rapid ISC from S_1 to T_1 and radiative decay from
23 T_1 to the ground state (usually in the microsecond timescale regime). Because of the presence of
24 these heavy atoms, spin-orbit coupling is usually large in phosphorescent emitters allowing for strong
25 mixing between singlet and triplet excited states, while it is relatively weak (on the order of tenths or
26 hundredths of meV) for TADF emitters made only of light elements. Still, the RISC mechanism is
27 expected to be mainly driven by spin-orbit coupling with a small contribution of hyperfine coupling,
28 as evidenced by electron paramagnetic resonance measurements⁹. This is further supported by
29 transient electron spin resonance (TrESR) on 2CzPN and 4CzIPN carbazoyl-dicyanobenzene based
30 TADF emitters, for which the observed absorption and emission patterns are characteristic of a spin-
31 orbit-driven ISC mechanism. Up to now, a systematic comparison between the different software
32 and models has not been carried out yet, although it was shown that the full Breit-Pauli model and
33 its mean field approximation lead to very similar spin-orbit coupling matrix elements for organic
34 dyes⁶³. Already in the 60s, Mostafa El-Sayed⁶⁴ highlighted the fact that spin-orbit coupling is
35 vanishing when (R)ISC takes place between excited states with identical π - π^* character. This is
36 because the change in spin angular momentum must be compensated by a corresponding change in
37 angular orbital momentum so that total angular momentum is conserved. As a result, only excited
38
39
40
41
42
43
44
45
46
47
48
49
50
51
52
53
54
55
56
57
58
59
60

states with different spatial wavefunctions couple through spin-orbit coupling. A textbook example is benzophenone that sustains $n-\pi^*$ and $\pi-\pi^*$ electronic excitations coupled through large spin-orbit matrix elements⁶⁵. Recently, this concept was put in practice in the context of TADF materials by associating the magnitude of the spin-orbit coupling to the difference in the nature of these excited states calculated based on the difference of normalized overlap between attachment/detachment densities, $\Delta\Phi_S$, between S_1 and T_1 . $\Delta\Phi_S$ was calculated on molecular conformations taken from an amorphous morphology of pure films of 2CzPN and 4CzIPN. Spin-orbit matrix elements are found to correlate approximately linearly with $\Delta\Phi_S$, becoming vanishingly small for $\Delta\Phi_S=0$, namely in the case where S_1 and T_1 are nearly degenerate ($\Delta E_{ST}\sim 0$) and exhibit both a strong and identical CT character, in line with the El-Sayed rules. Interestingly, because of its overall larger $\Delta\Phi_S$ offset, spin-orbit coupling is larger for 2CzPN than for 4CzIPN (see Figure 4b). Most importantly, we note that in the case of the carbazole derivatives studied in ⁷ spin-orbit coupling and ΔE_{ST} have antagonistic evolution, such as a trade-off has to be found in order to maximize the rate of RISC (see Figure 4a).

Most importantly, we note that spin-orbit coupling and ΔE_{ST} have antagonistic evolution, such as a trade-off has to be found in order to maximize the rate of RISC (see Figure 3a).

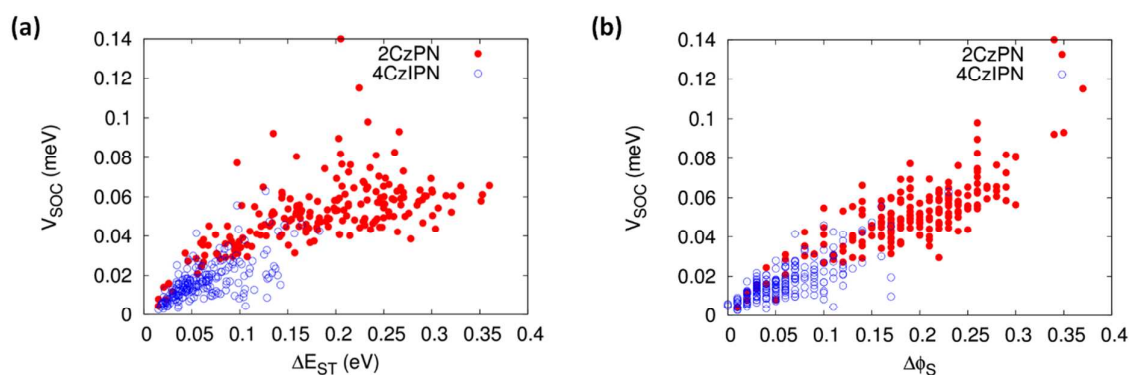


Figure 4: Spin-orbit coupling as a function of **a)** ΔE_{ST} and **b)** $\Delta\Phi_S$ in 2CzPN (blue data) and 4CzIPN (red data), as sampled from a realistic amorphous morphology simulated with molecular dynamics. The approximately linear correlation between V_{SOC} and $\Delta\Phi_S$ follows from the El Sayed rules, while the relationship between V_{SOC} and ΔE_{ST} highlights the need for a trade-off between different parameters for the optimization of TADF performances. Reprinted with permission from reference¹⁰. Copyright 2017 by the American Physical Society.

Two different internal conversion mechanisms with contrasting effects are considered here. On the one hand, the reverse IC in the triplet manifold of excited states which is a thermally-activated process, is expected to assist RISC by promoting the formation of higher-lying triplet excited states, from which the conversion to the singlet manifold might occur more efficiently because it is

1
2
3 associated with a larger exergonic character. This interconversion channel is expected to compete
4 with the direct conversion from T_1 to S_1 and features smaller activation energies⁶⁶. On the other
5 hand, non-radiative recombination to the ground state should take place mainly from S_1 and
6 contribute as the main monomolecular pathway to molecular excitation loss. Even though the two IC
7 processes described above involve excited states of different spin multiplicities, the initial and final
8 states are in both cases coupled through non-adiabatic couplings. The rate of internal conversion has
9 been calculated in triphenylamine-thiadiazole molecule using a Fermi Golden rule formalism and
10 considering non-adiabatic couplings for all relevant vibrational normal modes⁶⁷. This approach,
11 however, breaks down in the case internal conversion occurs at conical intersections, points of
12 degeneracy between electronic states acting as dynamic funnels for radiationless transitions^{68,69}.

13
14
15
16
17
18
19 In an OLED device, at high current, i.e. high hole and electron densities, triplets start accumulating in
20 the device. Bimolecular processes such as triplet-triplet or triplet-polaron annihilation might occur,
21 leading to an undesired roll-off behavior⁷⁰. So far, no mechanistic picture has been proposed for
22 these processes in the context of TADF materials. Triplet-triplet annihilation can proceed either via a
23 virtual CT state or through a two-electron exchange mechanism, similarly to its reverse process,
24 singlet fission⁷¹. The first attempts to include both processes in a device-like Kinetic Monte Carlo
25 simulation have been based on phenomenological grounds considering that triplet-triplet (triplet-
26 polaron) annihilation takes place when two triplet excitations (a triplet excitation and a charge)
27 occupy neighboring sites⁷². Assessing annihilation rates from first principles remains very challenging
28 since these processes involve the transient formation of high-lying electronic excitations with
29 multiple-excitation character, the description of which demands highly correlated quantum-chemical
30 methods often difficult to handle for large-size TADF emitters. A further challenge is that, since
31 annihilation is a bimolecular process, its theoretical investigation requires the knowledge of the
32 microscopic arrangement of emitters, so a further layer of calculations, as detailed in the next
33 paragraphs.

34
35
36
37
38
39
40
41
42
43
44 With respect to the gas phase or implicit solvent calculations described so far, a step further towards
45 the realistic modeling of TADF materials consists in taking into account explicitly the presence of
46 surrounding host molecules. This is possible via a simple two-step multiscale scheme, by first
47 employing classical (i.e. molecular mechanics) force fields and Molecular Dynamics (MD) or Monte
48 Carlo (MC) simulations to produce a realistic guess of the emitting layer morphology (see Figure 1 for
49 a simplified scheme of a multilayer OLED architecture),⁷³ and then performing electronic structure
50 calculations on single molecules or clusters extracted from the simulated trajectories. This approach
51 is considerably more expensive than a pure quantum mechanical-(QM-)based study, but its higher
52
53
54
55
56
57
58
59
60

1
2
3 computational cost is compensated by the number of additional important effects occurring in real
4 devices that can be accounted for, namely: i) sampling of many molecular geometries with a
5 probability of occurrence depending on temperature (Boltzmann-weighted); ii) conformational
6 changes and freezing induced by the solid matrix; and iii) inclusion of polarization and electrostatic
7 effects. Besides, simulations predict the orientation distribution of the emitters and, more generally,
8 provide the molecular positions of carriers and emitters, which are fundamental ingredients for
9 device modeling, and in particular for kinetic simulations of electronic processes.⁷⁴
10
11
12
13

14 Note that emitting layers are typically (meta)stable, disordered or partially ordered glasses, and host
15 and emitter molecules themselves (Figure 1) have characteristic of organic glass-formers, being often
16 constituted of a few, nonlinear rigid aromatic units interconnected by single rotatable bonds,
17 allowing thus for a relatively large number of stable conformations. There are at least three routes to
18 simulate amorphous morphologies of emissive layers, all of them essentially out of thermodynamic
19 equilibrium. The simplest scheme starts with an NPT-ensemble MD simulation at temperatures and
20 pressure high enough to obtain a fluid mixture of the desired composition, and subsequently cools
21 the sample at room temperature and equilibrates it until average volume and total energy appear
22 stable in time.^{10,75} A second, more costly approach imitates solvent annealing process, by starting
23 from a concentrated solution of the target materials equilibrated at ambient conditions, from which
24 molecules of solvent are progressively removed until a dry film is obtained. More recently, MD or MC
25 simulations in which molecules are progressively inserted in the system and landed on a substrate, a
26 scheme pioneered by some of us for the vapor deposition of organic crystalline semiconductors,^{76,77}
27 have gained increasing popularity in the OLED research field.⁷⁸⁻⁸¹ The origin of this trend is two-fold:
28 on the one hand, real TADF-based active layers are in fact prepared most often by co-deposition of
29 (at least) one host semiconductor and a guest TADF emitter,⁸² and on the other hand, since these
30 films are amorphous, it is difficult to validate the simulation results versus experimental structural
31 data, and it is tempting to believe that mimicking the experimental process could improve the quality
32 of the predictions. Indeed, one of the open questions in the field is how important is the simulation
33 procedure in determining the final morphology, and in turn how does it influence the calculated
34 electronic properties. Experimentally, there is a large body of evidence suggesting that vapor-
35 deposited systems are in general more stable and dense than spin-coated ones prepared by solvent
36 evaporation⁸² or freezing from the liquid phase;⁸³ however the exact shape of the potential energy
37 landscape (see scheme in Figure 5a for a pure material) not only does depend on the chemical nature
38 of the host-guest system but also on their relative concentration.
39
40
41
42
43
44
45
46
47
48
49
50
51
52
53
54
55
56
57
58
59
60

A further important result has recently emerged both from experiments^{78,84,85} and simulations:^{78–81} vapor deposited glasses can be to some extent orientationally anisotropic or, in other words, the orientation of the emitters in the active layer is not completely random. Since the specific orientation of emitter transition dipoles can strongly impact the outcoupling efficiency,^{86,87} it would be desirable to employ computer simulations in designing materials and setups apt at precisely controlling the orientation of the dyes, and then the direction of emitted light, in order to maximize the light output. The insurgence of anisotropy has been attributed to multiple factors, ranging from van der Waals interactions to dipole-dipole interactions and kinetic effects. These may be again system-dependent, but regardless of specific effects, it appears clear that a critical role is played by the orientation of the molecules at the growing interface with vacuum, as depicted in Figure 5b. Unfortunately, the current lack of knowledge about the relationship between all the simulation parameters (e.g. models, rates, temperatures, times, etc.) and the morphology obtained, so far does not allow to establish how general are the above-mentioned effects and to which extent they could be applicable to experimental results. Therefore, more systematic studies in this direction are urgent.

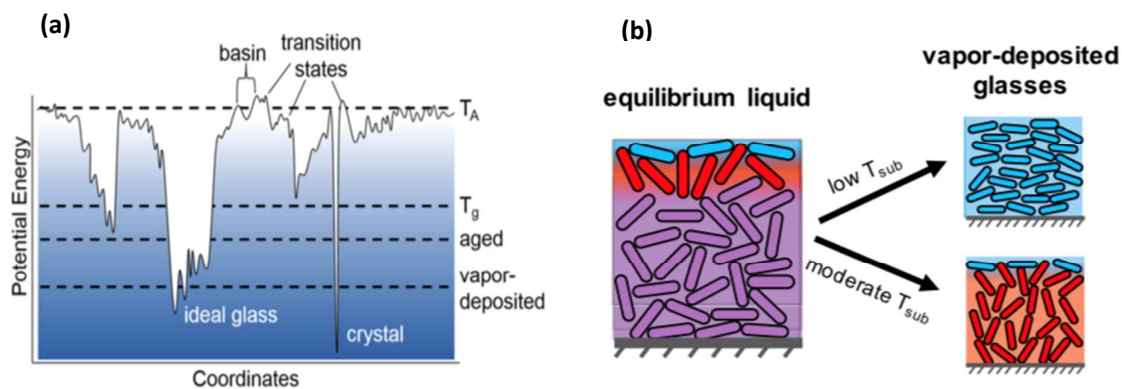


Figure 5: a) Schematic representation of the potential energy landscape of a glass forming system. T_A is the temperature where non-Arrhenius dynamics are first observed in the liquid. Upon cooling at a constant rate, a temperature is reached at which molecular motions freeze and a glass is formed (glass transition temperature T_g). Aging slightly below T_g allows some equilibration and lowers the potential energy. For some systems, much lower energies can be reached by physical vapor deposition with respect to aging or slow cooling. b) Possible origin of anisotropic molecular packing in vapor-deposited glasses of a rod-like molecule for which the free surface of the equilibrium liquid is anisotropic.^{78,88} The substrate temperature T_{sub} determines the depth to which structure at the surface can equilibrate during deposition. The lowest portion of the growing film becomes trapped by further deposition. Also the interface with the solid substrate can be in principle anisotropic. Reprinted from reference⁸³, with the permission of AIP Publishing.

1
2
3 Another, maybe unavoidable, problem in comparing simulations and experiments is the enormous
4 gap between the time scales accessible to simulations (microseconds) and the ones employed in the
5 lab (minutes, hours). This difference might shift the balance between kinetic and thermodynamic
6 effects, and may hamper the successful application of computer simulations to systems in which this
7 balance is delicate. Concerning instead length scales, the mismatch between reality and atomistic
8 models is much narrower, hundreds of nanometers versus tens or so. To reach the device scale,
9 coarse-grained models can be employed,^{78,89} with the main disadvantage of some extra effort for the
10 parameterization and complicated backmapping schemes to revert to the fully atomistic morphology,
11 needed for electronic structure calculations. United-atom force fields can be an effective
12 compromise, since the reduced number of centers allows a CPU time speed-up of about one order of
13 magnitude⁹⁰ and the backmapping to a full atom model is straightforward. Focusing on full-atom
14 models, there is a raising awareness that the use of classical force field geometries for QM
15 calculations may lead to uncontrolled approximations and systematic errors in the evaluation of
16 electronic properties, e.g. S_0 and T_1 energies.^{10,75} In order to minimize this source of error, it would
17 be beneficial to employ, in future studies, non-transferable force fields specifically tailored for
18 reproducing not only the QM optimized geometry, but also the vibrational frequencies in the
19 electronic state of interest.⁹¹

20
21 Radiative emission cross-sections, also quantified through the oscillator strength, are often very
22 small in TADF molecules with close to orthogonal donor and acceptor moieties in their ground- or
23 excited-state optimized geometries (see Figure 6b). Unless counterbalanced by specific
24 intramolecular interactions such as hydrogen-bonds,⁶¹ most TADF molecules usually feature a
25 twisted equilibrium conformation, which inevitably leads to a small overlap between the frontier π -
26 conjugated orbitals of the donor and acceptor moieties. Fortunately, in TADF emitters based on D
27 and A moieties connected through single bond, soft torsional modes are easily activated, generating
28 a large spectrum of conformations at room temperature^{4,7} (see Figure 6a). These display significantly
29 different absorption/emission energies and associated ΔE_{ST} values as the nature of the lowest singlet
30 and triplet excited states (as probed through Φ_S) varies in time and space (see Figures 6c and 6d).
31 Thermal excitation of these soft vibrational modes also results in broad and unstructured absorption
32 and emission spectra. Thermal motion around the twisted equilibrium structures has a positive
33 impact on luminescence, as it allows to sample conformations with larger overlap between the
34 electron and hole wavefunctions, *i.e.* also larger oscillator strengths and radiative decay rates.²⁰ In
35 this case, emission of the TADF materials appears as a vibrationally-assisted process strongly coupled
36 to soft (low-frequency) torsional modes.⁷

1
2
3 Also the RISC process, as claimed by Monkman and coworkers,³ can be seen as a spin-vibronic
4 mechanism where spin mixing is dynamically gated by conformational fluctuations triggered by low-
5 energy torsional modes. The influence of torsional modes on excited-state dynamics is two-fold: (i) it
6 brings excited states of the same spin multiplicity closer to each other, enhancing non-adiabatic
7 coupling between the lowest singlet (triplet) excited states;⁹² (ii) it affects dynamically the nature of
8 the singlet and triplet excited states involved in the TADF process in a way that the thermally-
9 averaged spin-orbit coupling is enhanced compared to its value at the equilibrium geometry.^{67,92} The
10 role of vibrations on TADF dynamics can be modeled using different formalisms, either based on non-
11 adiabatic molecular dynamics, such as mixed quantum-classical surface hopping methods⁹³ or full
12 quantum wavepacket propagation simulations,⁹⁴ or relying on rate expressions derived from time-
13 dependent second-order perturbation theory (Fermi Golden Rule).^{67,92} These approaches usually
14 include a set of preselected intramolecular vibrational modes for which the frequencies and
15 displacements (electron-phonon couplings) are computed from first-principles. Alternatively, one can
16 resort to MD simulations that allow sampling all vibrational modes classically, being intra- or inter-
17 molecular in origin, at once. In the case of low-frequency vibrations, classical and quantum
18 approximations yield similar results for thermally averaged spin-orbit coupling and ΔE_{ST} values.⁹⁵ The
19 reorganization energy associated with high-frequency vibrations, *i.e.* mostly bond stretching, can be
20 obtained from ground- and excited-state geometry optimization of the isolated molecules. These
21 modes steer temperature-independent quantum tunneling effects and can be easily incorporated
22 into rate expressions for ISC and RISC. For instance, by a careful analysis of the time evolution of the
23 dihedral angles in 2CzPN and 4CzIPN, a characteristic time scale of about 1 ps has been inferred. This
24 is fast compared to RISC, hence a large portion of the dihedral angles distribution is explored by the
25 molecule before upconversion takes place, which confirms the truly dynamic nature of the RISC
26 process. Considering thermally-averaged spin-orbit coupling and ΔE_{ST} for the specific case of 4CzIPN,
27 (R)ISC rates calculated within the semi-classical Marcus theory were found to be in excellent
28 agreement with experimental data.¹⁰

29
30
31 To close this discussion, we would like to briefly refer to studies pointing to the role of 'hard' modes.
32 For instance, it has been shown that the displacement along a C=O stretching mode on the donor
33 moiety of a xanthone-acridine D-A complex is able to bring in near resonance triplet ³CT and ³LE
34 states, from which efficient RISC to ¹CT proceeds.⁹⁶ Similarly, highly correlated wavefunction based
35 calculations in carbene-metal-amide complexes suggest that the dynamic red shift observed
36 experimentally is associated with changes in the carbon-nitrogen bond length and metal-carbon-
37 nitrogen bond angle within the carbene-metal-amide three-center core. Very interestingly, these
38 changes reduce ΔE_{ST} , while keeping unaffected the spin-orbit coupling and emission transition dipole
39
40
41
42
43
44
45
46
47
48
49
50
51
52
53
54
55
56
57

moment from the singlet excited state, at odds with the initially proposed rotationally-assisted upconversion mechanism.⁴⁵

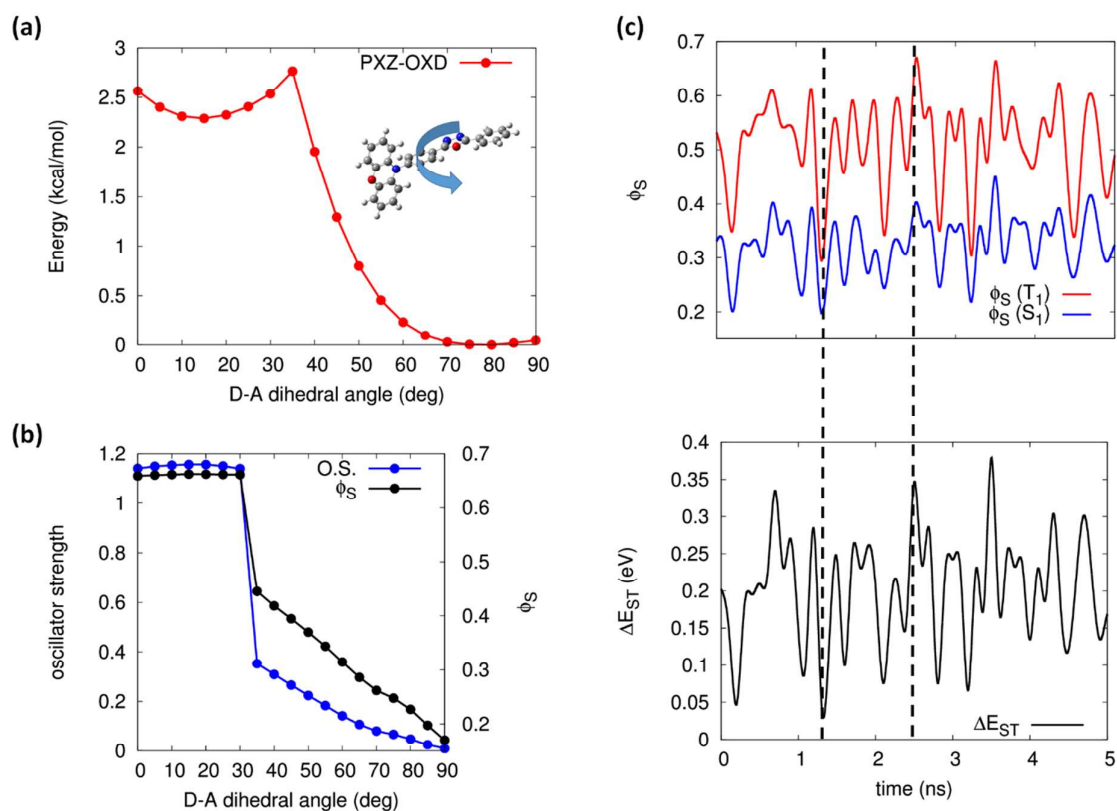


Figure 6: (a) Torsional energy profiles calculated at the PBE0-D3(BJ)/6-31G(d,p) level of theory with the PCM module for solvent (toluene) for PXZ-OXD. (b) Variation of ΔE_{ST} and oscillator strength (O.S) as a function of the D-A torsion angle. (c) Time evolution of the $\Phi_S(S_1)$ and $\Phi_S(T_1)$ from electronic structure calculations performed along a molecular dynamics trajectory for 2CzPN. (d) Time evolution of the ΔE_{ST} for 2CzPN. Vertical dashed lines highlight that ΔE_{ST} is the largest (smallest) when the difference in $\Phi_S(S_1)$ and $\Phi_S(T_1)$ is the largest (the smallest). Reproduced from Ref.⁷ with permission from The Royal Society of Chemistry. Reprinted and adapted with permission from reference¹⁰. Copyrights 2017 by the American Physical Society.

Environmental effects are known to have a major impact on molecular excitations of charge transfer character, yet the implications on ΔE_{ST} in TADF emitters has started to be appreciated only recently. The role of the environment is particularly subtle and important in systems where singlet and triplet excitations of CT and/or LE character are all close in energy and compete, while the energy window interesting for applications is of few tens of meV. Viable computational strategies consist in QM/MM approaches, where the TADF emitter (QM system) is embedded in a classical medium that can be

1
2
3 described either with PCM or with discrete schemes of atomistic resolutions. Both approaches have
4 advantages and limitations that we briefly discuss in the following.

5
6 In this context, Brédas and coworkers systematically employed the PCM in their TD-DFT
7 investigations of singlet-triplet splitting and spin-orbit matrix elements for different TADF
8 molecules.^{14,56} Sun et al. specifically addressed the effect of the dielectric constant (ϵ) on the nature
9 of the excited states and on the single-triplet splitting by using optimally tuned range-separated
10 hybrid functionals, whose range separation parameter ω was optimized for each value of ϵ .⁹⁷ These
11 calculations highlighted the role of the medium polarizability in stabilizing electronic configurations
12 with large CT character, in turn affecting the CT-LE hybridization in singlet and triplet excitations. For
13 instance, dipolar D-A molecules such as TXO-TPA and TXO-PhCz, which in the gas phase are
14 prescribed to feature large ΔE_{ST} (ca. 0.5 eV) as a result of the large LE character of T_1 , become
15 interesting for TADF applications in a typical organic matrix with $\epsilon \sim 3$. Indeed the medium polarization
16 leads to excitations with large CT character and nearly non-overlapping hole and electron clouds and
17 ΔE_{ST} below 0.1 eV.⁹⁷ Marian *et al.*⁴⁴ proposed a reinterpretation of the emission observed for
18 carbene-metal-amide in both solution and film based on a combination of DFT/MRCI and PCM.
19 Especially, they showed that solvent reorganization has to be taken into account when computing
20 the delayed fluorescence spectrum, while it is not required when discussing prompt fluorescence
21 occurring at early-timescale. Practically speaking, one needs to consider the relaxed density matrix of
22 the excited state to calculate the solvent reaction field. Delayed fluorescence appears to be red-
23 shifted in comparison the prompt one in agreement with experiment. However, in glassy films, such
24 a treatment is not needed because the medium reorientation is sterically hindered so that delayed
25 fluorescence appears to be blue-shifted compared to solution. Along the same line, Penfold *et al.*⁷⁵
26 have highlighted through a combination of MD and TD-DFT calculations that a blue shift in the
27 delayed emission of D-A TADF emitters in films at the longest timescale does not result from host
28 reorganization, and thus on specific host-guest interaction, but rather from a distribution of CT states
29 with different emission energies. The prompt fluorescence is essentially governed by the higher-
30 energy CT states that exhibit the largest hole-electron wavefunction overlap and therefore also
31 oscillator strength. As for the delayed fluorescence, the early part of the signal appears to be red-
32 shifted in comparison to the prompt fluorescence since RISC occurs first through the lower-energy CT
33 states that minimize ΔE_{ST} . The late delayed fluorescence component then occurs through higher-lying
34 but more emissive CT states, thereby rationalizing the blue-shift observed.

35
36
37
38
39
40
41
42
43
44
45
46
47
48
49
50
51
52
53 Beyond PCM, atomistic polarizable models aim at describing excitations of molecules in their specific
54 environment, usually an amorphous matrix blending the charge transporting material and other
55 emitters. Atomistic simulations of such blends are a prerequisite for these approaches, which also
56
57

allow for the sampling over a statistical collection of molecule-environment configurations. Our group adopted this route to study environmental effects in carbazoyl-dicyanobenzene based TADF emitters, 2CzPN and 4CzIPN, employing atomistic microelectrostatic models parameterized from first principles.¹⁰ These calculations showed that the medium polarization, modeled with mutually interacting anisotropic polarizabilities, reacts differently to states of different CT character (see Figure 7a). For instance, 2CzPN shows a singlet excitation S_1 that has larger CT character than the triplet T_1 , and thus a larger electrical dipole, resulting in a stronger stabilization of the former by the environment polarization, finally leading to a reduction in ΔE_{ST} (see Figure 7b). This provides a general mechanism through which the embedding medium compensates for large ΔE_{ST} established at the molecular level, leading in some cases to negative ΔE_{ST} values. In addition, atomistic models do also account for the fact that molecules are distorted in real morphologies and experience the inhomogeneous electrostatic potential of the neighborhood. These phenomena affect the energies of the excited states within both the singlet and the triplet manifold of states, leading to inhomogeneous broadening in the solid matrix and to broad distributions of ΔE_{ST} values. Such a disorder can also break the symmetry of the molecule (e.g. localizing the hole of a CT excitation on a given D carbazole unit) and, most interestingly, have a dynamic nature, i.e. lead to a modulation in time of the nature of the relevant states (CT-LE hybridization) and of the ΔE_{ST} .¹⁰

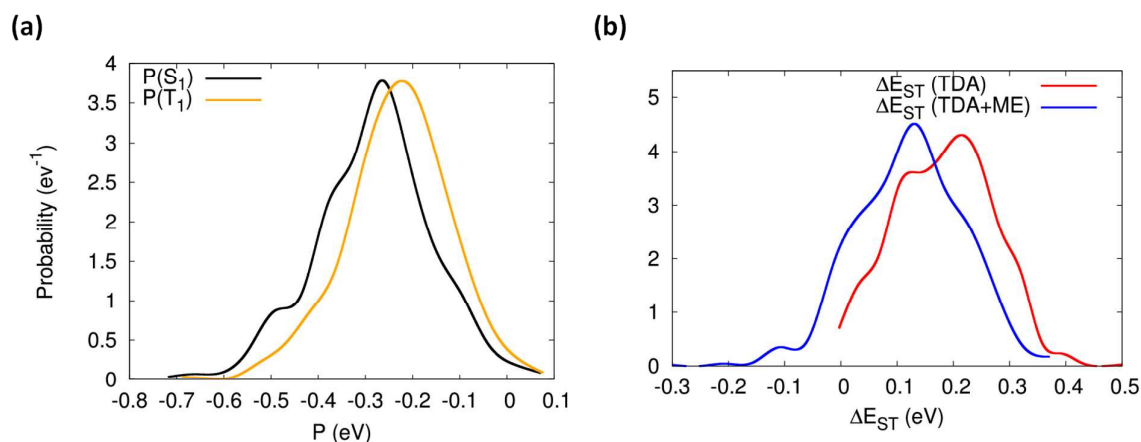


Figure 7: (a) Polarization energy distributions associated to S_1 and T_1 excited states. (b) Distributions of ΔE_{ST} . Red and blue lines correspond to TDA-PBE0 results in the vacuum and accounting for local dielectric effects, respectively. All data provided in this Figure refer to 2CzPN. Reprinted and adapted with permission from reference¹⁰. Copyright 2017 by the American Physical Society.

In summary, predictive modeling of TADF emitters requires an integrated multiscale approach able to capture the energetics and the dynamics of electronic excitations in realistic morphologies of OLEDs emitting layers. In combination with state-of-the-art experimental investigations (optical spectroscopy and device characterization), computational studies have already shed light on some key features of TADF, including:

- The excited states involved in TADF often feature mixed CT and LE character.
- The host influences ΔE_{ST} through conformational and dielectric effects.
- RISC and light emission are dynamic processes assisted by intramolecular vibrations.

While some of the items above remain open to discussion, as they are likely material-specific, they also prompt new questions and challenges that need to be addressed when designing the next generation of TADF emitters. For instance, can one tune the nature of the excited states involved in the TADF process in order to speedup RISC? Can one take advantage of environmental effects to design molecules with negative ΔE_{ST} ? Can we expand the modeling approaches in order to account for all the mono- and bi-molecular radiative and non-radiative processes taking place in TADF-based OLEDs and identify host-guest combinations that would minimize annihilation and maximize pure and color-tunable light emission?

Clearly the answer to these questions can only be obtained in the scope of a multifaceted theoretical framework, where molecular and material properties are conjointly addressed and optimized. More specifically, we would like to end this perspective with modeling challenges inspired by a few selected opportunities from recent experimental investigations:

- Hyperfluorescent OLEDs.⁹⁸ Here, TADF molecules act mostly as assistant dopants that drive the excitations towards a dye with narrow-line singlet emission. To further improve what is referred to as the 4th generation OLEDs, a microscopic picture for the diffusion of singlet and triplet excitations relevant to TADF is definitively needed. This would require going beyond the widely used Förster model for weakly dipole-allowed CT singlets and including both exchange and superexchange interactions for triplets.^{99–101}
- Highly emissive TADF emitters. Architectures sustaining multi-resonance effects^{28,102,103} have the potential to solve the conundrum of large singlet radiative decay rates despite small exchange energies. A proper description of the singlet and triplet excitations in these molecules calls for the inclusion of high-order electronic correlation effects, difficult to capture using conventional TD-DFT methods.
- Exciplexes. Despite considerable efforts to establish them as viable technology for OLED applications, exciplexes, namely emissive D-A intermolecular CT states, have been

1
2 investigated in only very few computational studies.^{104,105} This is surely related to the
3 weakness of intermolecular interactions in organics resulting in the large configurational
4 space explored by the D and A molecules that can adopt multiple relative orientations.
5 Besides sampling issues, another timely question relates to the quantum-mechanical effect
6 driving RISC in exciplexes, with scenarios based on either spin-orbit or hyperfine field
7 couplings proposed in the literature.^{104,106} Note that recent studies of crystalline
8 multichromophoric materials, composed on a mixed stack of 1:1 D-A molecules, are
9 particularly interesting in this context, too.^{107,108}
10
11
12
13
14
15

16 As a last note, we would like to stress that, as highlighted in this perspective, modeling of TADF is a
17 complex endeavor and we warn the community about the potential pitfalls of 'black box' calculations
18 using standard approaches. While these might provide a useful first screening, we believe that the
19 field of computational modeling has now reached a maturity level that allows for a truly first-
20 principles description of TADF emitters and hope this perspective will guide modelers and
21 experimentalists on finding their way to best practices in TADF.
22
23
24
25
26
27

28 **Biographical Sketches**

29
30
31 **Yoann Olivier** obtained a Ph.D. from the University of Mons in 2008. From 2009 to 2013, he held a
32 postdoctoral fellowship from Belgian National Fund for Scientific Research (FNRS) and went on
33 postdoctoral stays with Prof. Claudio Zannoni at the University of Bologna and Prof. Henning
34 Siringhaus at the University of Cambridge. He is currently a research associate at the University of
35 Mons. His research interests deal with the understanding of electronic processes in organic
36 conjugated and 2D materials, using a multiscale approach combining quantum-chemical methods,
37 Monte Carlo approach and molecular dynamics simulations.
38
39
40
41
42
43

44 **Juan-Carlos Sancho-Garcia** obtained a Ph.D. in Quantum Chemistry in 2001 at the University of
45 Alicante, followed by a postdoctoral stay (2002-2004) at the Laboratory for Chemistry of Novel
46 Materials in Mons, Belgium. He returned to Alicante as a 'Ramon y Cajal' research fellow and
47 received a permanent position in 2010 in the Dept. of Physical Chemistry. His work integrates the
48 development of more accurate DFT methods with applications to the field of Organic Electronics to
49 elucidate structure-property relationships."
50
51
52
53
54
55
56
57
58
59
60

1
2
3 **Luca Muccioli** is assistant professor of Physical Chemistry at the University of Bologna (Italy). He
4 earned a Ph.D. in Chemical Sciences from University of Bologna in 2003, under the supervision of
5 Prof. Claudio Zannoni, with a thesis on atomistic computer simulations of liquid crystals.

6
7 From 2003 to 2014 he was postdoctoral researcher at the University of Bologna, and from 2014 to
8 2016 assistant professor at the Institut des Sciences Moléculaires of the University of Bordeaux
9 (France). His research interests concern the application of computational chemistry techniques to the
10 study of the physico-chemical properties of organic materials, with particular focus on the prediction
11 of structural and electronic properties of liquid crystals and organic semiconductors through
12 multiscale approaches
13
14
15
16
17

18 **Gabriele D'Avino** received his Ph.D. in Materials Science at the University of Parma in 2010. After a
19 postdoctoral research position at the University of Bologna, and two Marie Curie fellowships at the
20 University of Liege and at the University of Mons, he is currently CNRS associate researcher at the
21 Institut Institut Néel, Grenoble. His research focuses on the multiscale modeling of organic functional
22 materials, merging quantum and classical techniques.
23
24
25
26
27

28 **David Beljonne** got his PhD in Chemistry at the University of Mons-Hainaut in 1994. After post-
29 doctoral stays at the Universities of Cambridge (with Prof. Friend) and Rochester (with Prof.
30 Mukamel), he is now a Research Director of the Belgian National Science Foundation (FNRS) and
31 Professor at the University of Mons. He is also a Visiting Principal Research Scientist at the Georgia
32 Institute of Technology in Atlanta. His research activities deal with the modeling of semiconducting
33 materials for energy applications.
34
35
36
37
38

39 **PULL QUOTES**

40
41

- 42 (i) Can we predict the nature of the excited states and tune the primary chemical structure of
43 TADF emitters in order to maximize the efficiency of upconversion and light emission in
44 TADF-based OLEDs?
45
46
47
48 (ii) How important is the simulation procedure in determining the final morphology, and in turn
49 how does it influence the calculated electronic properties?
50
51
52
53 (iii) How can we design *in silico* TADF emitters that yield the right orientation in the solid-state
54 matrix to maximize light outcoupling?
55
56
57
58
59
60

- 1
2
3 (iv) How much torsional dynamics is affected by the host-guest interaction? How does it affect
4 the efficiency of TADF?
5
6
7 (v) Polarization medium effects are stabilizing CT states with respect to LE states. Could we
8 possibly target the right combination of host and guest in order to get negative ΔE_{ST} ?
9
10
11 (vi) Should we freeze-out the motion of triplet excitations in TADF materials in order to reduce
12 annihilation processes?
13
14
15

16 Acknowledgments

17
18 The work in Mons was supported by the Belgian National Science Foundation, F.R.S.-FNRS.
19 Computational resources have been provided by the Consortium des Équipements de Calcul Intensif
20 (CÉCI), funded by F.R.S.-FNRS under Grant No. 2.5020.11 as well as the Tier-1 supercomputer of the
21 Fédération Wallonie-Bruxelles, infrastructure funded by the Walloon Region under the grant
22 agreement n1117545. The research in Bologna, Grenoble and Mons is also through the European
23 Union's Horizon 2020 research and innovation program under Grant Agreement No. 646176
24 (EXTMOS project). GD would like to thank Prof. Xavier Blase for discussions. JC, LM and YO
25 acknowledge discussion with Dr. Mónica Moral. DB and YO would like to thank Prof. Thuc Quyen
26 Nguyen and Brett Yurash for the fruitful collaboration on the 2CzPN and 4CzIPN study. DB is a FNRS
27 Research Director.
28
29
30
31
32
33
34

35 References

- 36
37 (1) Parker, C. A.; Hatchard, C. G. Triplet-Singlet Emission in Fluid Solutions. Phosphorescence of
38 Eosin. *Trans. Faraday Soc.* **1961**, *57*, 1894-1904.
39
40 (2) Uoyama, H.; Goushi, K.; Shizu, K.; Nomura, H.; Adachi, C. Highly Efficient Organic Light-
41 Emitting Diodes from Delayed Fluorescence. *Nature* **2012**, *492*, 234–238.
42
43 (3) Etherington, M. K.; Gibson, J.; Higginbotham, H. F.; Penfold, T. J.; Monkman, A. P. Revealing
44 the Spin–vibronic Coupling Mechanism of Thermally Activated Delayed Fluorescence. *Nat.*
45 *Commun.* **2016**, *7*, 13680.
46
47 (4) Dias, F. B.; Santos, J.; Graves, D. R.; Data, P.; Nobuyasu, R. S.; Fox, M. A.; Batsanov, A. S.;
48 Palmeira, T.; Berberan-Santos, M. N.; Bryce, M. R.; et al. The Role of Local Triplet Excited
49 States and D-A Relative Orientation in Thermally Activated Delayed Fluorescence:
50 Photophysics and Devices. *Adv. Sci.* **2016**, *3*, 1600080.
51
52 (5) Hosokai, T.; Matsuzaki, H.; Nakanotani, H.; Tokumaru, K.; Tsutsui, T.; Furube, A.; Nasu, K.;
53 Nomura, H.; Yahiro, M.; Adachi, C. Evidence and Mechanism of Efficient Thermally Activated
54
55
56
57
58
59
60

- 1
2
3 Delayed Fluorescence Promoted by Delocalized Excited States. *Sci. Adv.* **2017**, *3*, e1603282.
- 4 (6) Milián-Medina, B.; Gierschner, J. Computational Design of Low Singlet–triplet Gap All-Organic
5 Molecules for OLED Application. *Org. Electron.* **2012**, *13*, 985–991.
- 6
7 (7) Olivier, Y.; Moral, M.; Muccioli, L.; Sancho-García, J.-C. Dynamic Nature of Excited States of
8 Donor-Acceptor TADF Materials for OLEDs: How Theory Can Reveal Structure-Property
9 Relationships. *J. Mater. Chem. C* **2017**, *5*, 5718–5729.
- 10
11 (8) Wong, M. Y.; Zysman-Colman, E. Purely Organic Thermally Activated Delayed Fluorescence
12 Materials for Organic Light-Emitting Diodes. *Adv. Mater.* **2017**, *29*, 1605444.
- 13
14 (9) Schott, S.; McNellis, E. R.; Nielsen, C. B.; Chen, H. Y.; Watanabe, S.; Tanaka, H.; McCulloch, I.;
15 Takimiya, K.; Sinova, J.; Sirringhaus, H. Tuning the Effective Spin-Orbit Coupling in Molecular
16 Semiconductors. *Nat. Commun.* **2017**, *8*, 15200.
- 17
18 (10) Olivier, Y.; Yurash, B.; Muccioli, L.; D’Avino, G.; Mikhnenko, O.; Sancho-García, J. C.; Adachi, C.;
19 Nguyen, T.-Q.; Beljonne, D. Nature of the Singlet and Triplet Excitations Mediating Thermally
20 Activated Delayed Fluorescence. *Phys. Rev. Mater.* **2017**, *1*, 75602.
- 21
22 (11) Gómez-Bombarelli, R.; Aguilera-Iparraguirre, J.; Hirzel, T. D.; Duvenaud, D.; Maclaurin, D.;
23 Blood-Forsythe, M. A.; Chae, H. S.; Einzinger, M.; Ha, D.-G.; Wu, T.; et al. Design of Efficient
24 Molecular Organic Light-Emitting Diodes by a High-Throughput Virtual Screening and
25 Experimental Approach. *Nat. Mater.* **2016**, *15*, 1120–1127.
- 26
27 (12) Chen, X.-K.; Kim, D.; Brédas, J.-L. Thermally Activated Delayed Fluorescence (TADF) Path
28 toward Efficient Electroluminescence in Purely Organic Materials: Molecular Level Insight.
29 *Acc. Chem. Res.* **2018**, *51*, 2215–2224.
- 30
31 (13) Moral, M.; Muccioli, L.; Son, W.-J.; Olivier, Y.; Sancho-García, J. C. Theoretical Rationalization
32 of the Singlet–Triplet Gap in OLEDs Materials: Impact of Charge-Transfer Character. *J. Chem.*
33 *Theory Comput.* **2015**, *11*, 168–177.
- 34
35 (14) Sun, H.; Zhong, C.; Brédas, J. L. Reliable Prediction with Tuned Range-Separated Functionals of
36 the Singlet-Triplet Gap in Organic Emitters for Thermally Activated Delayed Fluorescence. *J.*
37 *Chem. Theory Comput.* **2015**, *11*, 3851–3858.
- 38
39 (15) Peng, Q.; Fan, D.; Duan, R.; Yi, Y.; Niu, Y.; Wang, D.; Shuai, Z. Theoretical Study of Conversion
40 and Decay Processes of Excited Triplet and Singlet States in a Thermally Activated Delayed
41 Fluorescence Molecule. *J. Phys. Chem. C* **2017**, *121*, 13448–13456.
- 42
43 (16) Schreiber, M.; Silva-Junior, M. R.; Sauer, S. P. A.; Thiel, W. Benchmarks for Electronically
44 Excited States: CASPT2, CC2, CCSD, and CC3. *J. Chem. Phys.* **2008**, *128*, 134110.
- 45
46 (17) Silva-Junior, M. R.; Schreiber, M.; Sauer, S. P. A.; Thiel, W. Benchmarks for Electronically
47 Excited States: Time-Dependent Density Functional Theory and Density Functional Theory
48 Based Multireference Configuration Interaction. *J. Chem. Phys.* **2008**, *129*, 104103.
- 49
50
51
52
53
54
55
56
57
58
59
60

- 1
2
3 (18) Jacquemin, D.; Wathelet, V.; Perpète, E. A.; Adamo, C. Extensive TD-DFT Benchmark: Singlet-
4 Excited States of Organic Molecules. *J. Chem. Theory Comput.* **2009**, *5*, 2420–2435.
5
6 (19) Loos, P.-F.; Scemama, A.; Blondel, A.; Garniron, Y.; Caffarel, M.; Jacquemin, D. A
7 Mountaineering Strategy to Excited States: Highly Accurate Reference Energies and
8 Benchmarks. *J. Chem. Theory Comput.* **2018**, *14*, 4360–4379.
9
10 (20) Mewes, J.-M. Modeling TADF in Organic Emitters Requires a Careful Consideration of the
11 Environment and Going beyond the Franck–Condon Approximation. *Phys. Chem. Chem. Phys.*
12 **2018**, *20*, 12454–12469.
13
14 (21) Hellweg, A.; Grün, S. A.; Hättig, C. Benchmarking the Performance of Spin-Component Scaled
15 CC2 in Ground and Electronically Excited States. *Phys. Chem. Chem. Phys.* **2008**, *10*, 4119-
16 4127.
17
18 (22) Jacquemin, D.; Duchemin, I.; Blondel, A.; Blase, X. Benchmark of Bethe-Salpeter for Triplet
19 Excited-States. *J. Chem. Theory Comput.* **2017**, *13*, 767–783.
20
21 (23) Noguchi, Y.; Sugino, O. High-Lying Triplet Excitons of Thermally Activated Delayed
22 Fluorescence Molecules. *J. Phys. Chem. C* **2017**, *121*, 20687–20695.
23
24 (24) Rangel, T.; Hamed, S. M.; Bruneval, F.; Neaton, J. B. An Assessment of Low-Lying Excitation
25 Energies and Triplet Instabilities of Organic Molecules with an *Ab Initio* Bethe-Salpeter
26 Equation Approach and the Tamm-Dancoff Approximation. *J. Chem. Phys.* **2017**, *146*, 194108.
27
28 (25) Weigend, F.; Häser, M.; Patzelt, H.; Ahlrichs, R. RI-MP2: Optimized Auxiliary Basis Sets and
29 Demonstration of Efficiency. *Chem. Phys. Lett.* **1998**, *294*, 143–152.
30
31 (26) Weigend, F. A Fully Direct RI-HF Algorithm: Implementation, Optimised Auxiliary Basis Sets,
32 Demonstration of Accuracy and Efficiency. *Phys. Chem. Chem. Phys.* **2002**, *4*, 4285–4291.
33
34 (27) Werner, H.-J.; Manby, F. R.; Knowles, P. J. Fast Linear Scaling Second-Order Møller-Plesset
35 Perturbation Theory (MP2) Using Local and Density Fitting Approximations. *J. Chem. Phys.*
36 **2003**, *118*, 8149–8160.
37
38 (28) Hatakeyama, T.; Shiren, K.; Nakajima, K.; Nomura, S.; Nakatsuka, S.; Kinoshita, K.; Ni, J.; Ono,
39 Y.; Ikuta, T. Ultrapure Blue Thermally Activated Delayed Fluorescence Molecules: Efficient
40 HOMO-LUMO Separation by the Multiple Resonance Effect. *Adv. Mater.* **2016**, *28*, 2777–2781.
41
42 (29) Brückner, C.; Engels, B. Benchmarking Singlet and Triplet Excitation Energies of Molecular
43 Semiconductors for Singlet Fission: Tuning the Amount of HF Exchange and Adjusting Local
44 Correlation to Obtain Accurate Functionals for Singlet–triplet Gaps. *Chem. Phys.* **2017**, *482*,
45 319–338.
46
47 (30) Nakagawa, T.; Ku, S.-Y.; Wong, K.-T.; Adachi, C. Electroluminescence Based on Thermally
48 Activated Delayed Fluorescence Generated by a Spirobifluorene Donor–acceptor Structure.
49 *Chem. Commun.* **2012**, *48*, 9580–9582.
50
51
52
53
54
55
56
57
58
59
60

- 1
2
3 (31) Cai, X.; Chen, D.; Gao, K.; Gan, L.; Yin, Q.; Qiao, Z.; Chen, Z.; Jiang, X.; Su, S.-J. "Trade-Off"
4 Hidden in Condensed State Solvation: Multiradiative Channels Design for Highly Efficient
5 Solution-Processed Purely Organic Electroluminescence at High Brightness. *Adv. Funct. Mater.*
6 **2018**, *28*, 1704927.
7
8
9 (32) Huang, S.; Zhang, Q.; Shiota, Y.; Nakagawa, T.; Kuwabara, K.; Yoshizawa, K.; Adachi, C.
10 Computational Prediction for Singlet- and Triplet-Transition Energies of Charge-Transfer
11 Compounds. *J. Chem. Theory Comput.* **2013**, *9*, 3872–3877.
12
13 (33) Jacquemin, D.; Perpète, E. A.; Ciofini, I.; Adamo, C.; Valero, R.; Zhao, Y.; Truhlar, D. G. On the
14 Performances of the M06 Family of Density Functionals for Electronic Excitation Energies. *J.*
15 *Chem. Theory Comput.* **2010**, *6*, 2071–2085.
16
17 (34) Hirata, S.; Head-Gordon, M. Time-Dependent Density Functional Theory within the Tamm–
18 Dancoff Approximation. *Chem. Phys. Lett.* **1999**, *314*, 291–299.
19
20 (35) Penfold, T. J. On Predicting the Excited-State Properties of Thermally Activated Delayed
21 Fluorescence Emitters. *J. Phys. Chem. C* **2015**, *119*, 13535–13544.
22
23 (36) Leininger, T.; Stoll, H.; Werner, H.-J.; Savin, A. Combining Long-Range Configuration
24 Interaction with Short-Range Density Functionals. *Chem. Phys. Lett.* **1997**, *275*, 151–160.
25
26 (37) Iikura, H.; Tsuneda, T.; Yanai, T.; Hirao, K. A Long-Range Correction Scheme for Generalized-
27 Gradient-Approximation Exchange Functionals. *J. Chem. Phys.* **2001**, *115*, 3540–3544.
28
29 (38) Yanai, T.; Tew, D. P.; Handy, N. C. A New Hybrid Exchange–correlation Functional Using the
30 Coulomb-Attenuating Method (CAM-B3LYP). *Chem. Phys. Lett.* **2004**, *393*, 51–57.
31
32 (39) Hait, D.; Zhu, T.; McMahon, D. P.; Van Voorhis, T. Prediction of Excited-State Energies and
33 Singlet–Triplet Gaps of Charge-Transfer States Using a Restricted Open-Shell Kohn–Sham
34 Approach. *J. Chem. Theory Comput.* **2016**, *12*, 3353–3359.
35
36 (40) Di, D.; Romanov, A. S.; Yang, L.; Richter, J. M.; Rivett, J. P. H.; Jones, S.; Thomas, T. H.; Abdi
37 Jalebi, M.; Friend, R. H.; Linnolahti, M.; et al. High-Performance Light-Emitting Diodes Based
38 on Carbene-Metal-Amides. *Science* **2017**, *356*, 159–163.
39
40 (41) Grimme, S.; Bannwarth, C. Ultra-Fast Computation of Electronic Spectra for Large Systems by
41 Tight-Binding Based Simplified Tamm-Dancoff Approximation (sTDA-xTB). *J. Chem. Phys.* **2016**,
42 *145*, 054103.
43
44 (42) Alipour, M.; Karimi, N. Dissecting the Accountability of Parameterized and Parameter-Free
45 Single-Hybrid and Double-Hybrid Functionals for Photophysical Properties of TADF-Based
46 OLEDs. *J. Chem. Phys.* **2017**, *146*, 234304.
47
48 (43) Lyskov, I.; Kleinschmidt, M.; Marian, C. M. Redesign of the DFT/MRCI Hamiltonian. *J. Chem.*
49 *Phys.* **2016**, *144*, 034104.
50
51 (44) Föllner, J.; Marian, C. M. Rotationally Assisted Spin-State Inversion in Carbene–Metal–Amides Is
52
53
54
55
56
57
58
59
60

- 1
2
3 an Artifact. *J. Phys. Chem. Lett.* **2017**, *8*, 5643–5647.
- 4 (45) Taffet, E. J.; Olivier, Y.; Lam, F.; Beljonne, D.; Scholes, G. D. Carbene–Metal–Amide Bond
5 Deformation, Rather Than Ligand Rotation, Drives Delayed Fluorescence. *J. Phys. Chem. Lett.*
6 **2018**, *9*, 1620–1626.
- 7
8 (46) Maschietto, F.; Campetella, M.; Frisch, M. J.; Scalmani, G.; Adamo, C.; Ciofini, I. How Are the
9 Charge Transfer Descriptors Affected by the Quality of the Underpinning Electronic Density? *J.*
10 *Comput. Chem.* **2018**, *39*, 735–742.
- 11
12 (47) Peach, M. J. G.; Benfield, P.; Helgaker, T.; Tozer, D. J. Excitation Energies in Density Functional
13 Theory: An Evaluation and a Diagnostic Test. *J. Chem. Phys.* **2008**, *128*, 044118.
- 14
15 (48) Peach, M. J. G.; Tozer, D. J. Illustration of a TDDFT Spatial Overlap Diagnostic by Basis Function
16 Exponent Scaling. *J. Mol. Struct. THEOCHEM* **2009**, *914*, 110–114.
- 17
18 (49) Guido, C. A.; Cortona, P.; Mennucci, B.; Adamo, C. On the Metric of Charge Transfer Molecular
19 Excitations: A Simple Chemical Descriptor. *J. Chem. Theory Comput.* **2013**, *9*, 3118–3126.
- 20
21 (50) Guido, C. A.; Cortona, P.; Adamo, C. Effective Electron Displacements: A Tool for Time-
22 Dependent Density Functional Theory Computational Spectroscopy. *J. Chem. Phys.* **2014**, *140*,
23 104101.
- 24
25 (51) Le Bahers, T.; Adamo, C.; Ciofini, I. A Qualitative Index of Spatial Extent in Charge-Transfer
26 Excitations. *J. Chem. Theory Comput.* **2011**, *7*, 2498–2506.
- 27
28 (52) Etienne, T.; Assfeld, X.; Monari, A. Toward a Quantitative Assessment of Electronic
29 Transitions' Charge-Transfer Character. *J. Chem. Theory Comput.* **2014**, *10*, 3896–3905.
- 30
31 (53) Campetella, M.; Maschietto, F.; Frisch, M. J.; Scalmani, G.; Ciofini, I.; Adamo, C. Charge
32 Transfer Excitations in TDDFT: A Ghost-Hunter Index. *J. Comput. Chem.* **2017**, *38*, 2151–2156.
- 33
34 (54) Savarese, M.; Guido, C. A.; Brémond, E.; Ciofini, I.; Adamo, C. Metrics for Molecular Electronic
35 Excitations: A Comparison between Orbital- and Density-Based Descriptors. *J. Phys. Chem. A*
36 **2017**, *121*, 7543–7549.
- 37
38 (55) Etienne, T.; Assfeld, X.; Monari, A. New Insight into the Topology of Excited States through
39 Detachment/Attachment Density Matrices-Based Centroids of Charge. *J. Chem. Theory*
40 *Comput.* **2014**, *10*, 3906–3914.
- 41
42 (56) Samanta, P. K.; Kim, D.; Coropceanu, V.; Brédas, J. L. Up-Conversion Intersystem Crossing
43 Rates in Organic Emitters for Thermally Activated Delayed Fluorescence: Impact of the Nature
44 of Singlet vs Triplet Excited States. *J. Am. Chem. Soc.* **2017**, *139*, 4042–4051.
- 45
46 (57) Köhler, A.; Beljonne, D. The Singlet–Triplet Exchange Energy in Conjugated Polymers. *Adv.*
47 *Funct. Mater.* **2004**, *14*, 11–18.
- 48
49 (58) Richert, S.; Tait, C. E.; Timmel, C. R. Delocalisation of Photoexcited Triplet States Probed by
50 Transient EPR and Hyperfine Spectroscopy. *J. Magn. Reson.* **2017**, *280*, 103–116.
- 51
52
53
54
55
56
57
58
59
60

- 1
2
3 (59) Barone, V. Structure, Magnetic Properties and Reactivities of Open-Shell Species From Density
4 Functional and Self-Consistent Hybrid Methods. In *Recent Advances in Computational*
5 *Chemistry*; 1995; pp. 287–334.
- 6
7 (60) Evans, E. W.; Olivier, Y.; Puttisong, Y.; Myers, W. K.; Hele, T. J. H.; Menke, S. M.; Thomas, T. H.;
8 Credgington, D.; Beljonne, D.; Friend, R. H.; et al. Vibrationally Assisted Intersystem Crossing
9 in Benchmark Thermally Activated Delayed Fluorescence Molecules. *J. Phys. Chem. Lett.* **2018**,
10 *9*, 4053–4058.
- 11
12 (61) Chen, X.-K.; Tsuchiya, Y.; Ishikawa, Y.; Zhong, C.; Adachi, C.; Brédas, J.-L. A New Design
13 Strategy for Efficient Thermally Activated Delayed Fluorescence Organic Emitters: From
14 Twisted to Planar Structures. *Adv. Mater.* **2017**, *29*, 1702767.
- 15
16 (62) Walker, T. E. H.; Richards, W. G. Molecular Spin–Orbit Coupling Constants. The Role of Core
17 Polarization. *J. Chem. Phys.* **1970**, *52*, 1311–1314.
- 18
19 (63) Alberto, M. E.; De Simone, B. C.; Mazzone, G.; Quartarolo, A. D.; Russo, N. Theoretical
20 Determination of Electronic Spectra and Intersystem Spin–Orbit Coupling: The Case of
21 Isoindole-BODIPY Dyes. *J. Chem. Theory Comput.* **2014**, *10*, 4006–4013.
- 22
23 (64) Lower, S. K.; El-Sayed, M. A. The Triplet State and Molecular Electronic Processes in Organic
24 Molecules. *Chem. Rev.* **1966**, *66*, 199–241.
- 25
26 (65) M. Klessinger, J. M. *Excited States and Photochemistry of Organic Molecules*; VCH Weinheim,
27 1995.
- 28
29 (66) Gibson, J.; Penfold, T. J. Nonadiabatic Coupling Reduces the Activation Energy in Thermally
30 Activated Delayed Fluorescence. *Phys. Chem. Chem. Phys.* **2017**, *19*, 8428–8434.
- 31
32 (67) Fan, D.; Yi, Y.; Li, Z.; Liu, W.; Peng, Q.; Shuai, Z. Solvent Effects on the Optical Spectra and
33 Excited-State Decay of Triphenylamine-Thiadiazole with Hybridized Local Excitation and
34 Intramolecular Charge Transfer. *J. Phys. Chem. A* **2015**, *119*, 5233–5240.
- 35
36 (68) Levine, B. G.; Martínez, T. J. Isomerization Through Conical Intersections. *Annu. Rev. Phys.*
37 *Chem.* **2007**, *58*, 613–634.
- 38
39 (69) Blancafort, L. Photochemistry and Photophysics at Extended Seams of Conical Intersection.
40 *ChemPhysChem* **2014**, *15*, 3166–3181.
- 41
42 (70) Murawski, C.; Leo, K.; Gather, M. C. Efficiency Roll-Off in Organic Light-Emitting Diodes. *Adv.*
43 *Mater.* **2013**, *25*, 6801–6827.
- 44
45 (71) Smith, M. B.; Michl, J. Singlet Fission. *Chem. Rev.* **2010**, *110*, 6891–6936.
- 46
47 (72) Coehoorn, R.; van Eersel, H.; Bobbert, P.; Janssen, R. Kinetic Monte Carlo Study of the
48 Sensitivity of OLED Efficiency and Lifetime to Materials Parameters. *Adv. Funct. Mater.* **2015**,
49 *25*, 2024–2037.
- 50
51 (73) Muccioli, L.; D’Avino, G.; Berardi, R.; Orlandi, S.; Pizzirusso, A.; Ricci, M.; Roscioni, O. M.;

- Zannoni, C. Supramolecular Organization of Functional Organic Materials in the Bulk and at Organic/Organic Interfaces: A Modeling and Computer Simulation Approach. *Top. Curr. Chem.* **2013**, *352*, 39–101.
- (74) Groves, C. Simulating Charge Transport in Organic Semiconductors and Devices: A Review. *Rep. Prog. Phys.* **2017**, *80*, 026502.
- (75) Northey, T.; Stacey, J.; Penfold, T. J. The Role of Solid State Solvation on the Charge Transfer State of a Thermally Activated Delayed Fluorescence Emitter. *J. Mater. Chem. C* **2017**, *5*, 11001–11009.
- (76) Muccioli, L.; D'Avino, G.; Zannoni, C. Simulation of Vapor-Phase Deposition and Growth of a Pentacene Thin Film on C60 (001). *Adv. Mater.* **2011**, *23*, 4532–4536.
- (77) D'Avino, G.; Muccioli, L.; Zannoni, C. From Chiral Islands to Smectic Layers: A Computational Journey Across Sexithiophene Morphologies on C 60. *Adv. Funct. Mater.* **2015**, *25*, 1985–1995.
- (78) Dalal, S. S.; Walters, D. M.; Lyubimov, I.; de Pablo, J. J.; Ediger, M. D. Tunable Molecular Orientation and Elevated Thermal Stability of Vapor-Deposited Organic Semiconductors. *Proc. Natl. Acad. Sci. USA* **2015**, *112*, 4227–4232.
- (79) Friederich, P.; Coehoorn, R.; Wenzel, W. Molecular Origin of the Anisotropic Dye Orientation in Emissive Layers of Organic Light Emitting Diodes. *Chem. Mater.* **2017**, *29*, 9528–9535.
- (80) Tonnelé, C.; Stroet, M.; Caron, B.; Clulow, A. J.; Nagiri, R. C. R.; Malde, A. K.; Burn, P. L.; Gentle, I. R.; Mark, A. E.; Powell, B. J. Elucidating the Spatial Arrangement of Emitter Molecules in Organic Light-Emitting Diode Films. *Angew. Chemie Int. Ed.* **2017**, *56*, 8402–8406.
- (81) Youn, Y.; Yoo, D.; Song, H.; Kang, Y.; Kim, K. Y.; Jeon, S. H.; Cho, Y.; Chae, K.; Han, S. All-Atom Simulation of Molecular Orientation in Vapor-Deposited Organic Light-Emitting Diodes. *J. Mater. Chem. C* **2018**, *6*, 1015–1022.
- (82) Shibata, M.; Sakai, Y.; Yokoyama, D. Advantages and Disadvantages of Vacuum-Deposited and Spin-Coated Amorphous Organic Semiconductor Films for Organic Light-Emitting Diodes. *J. Mater. Chem. C* **2015**, *3*, 11178–11191.
- (83) Ediger, M. D. Perspective: Highly Stable Vapor-Deposited Glasses. *J. Chem. Phys.* **2017**, *147*, 210901.
- (84) Komino, T.; Tanaka, H.; Adachi, C. Selectively Controlled Orientational Order in Linear-Shaped Thermally Activated Delayed Fluorescent Dopants. *Chem. Mater.* **2014**, *26*, 3665–3671.
- (85) Hasegawa, Y.; Yamada, Y.; Sasaki, M.; Hosokai, T.; Nakanotani, H.; Adachi, C. Well-Ordered 4CzIPN ((4s,6s)-2,4,5,6-Tetra(9-H-Carbazol-9-Yl)isophthalonitrile) Layers: Molecular Orientation, Electronic Structure, and Angular Distribution of Photoluminescence. *J. Phys. Chem. Lett.* **2018**, *9*, 863–867.
- (86) Schmidt, T. D.; Lampe, T.; Sylvinson M. R., D.; Djurovich, P. I.; Thompson, M. E.; Brütting, W.

- 1
2
3 Emitter Orientation as a Key Parameter in Organic Light-Emitting Diodes. *Phys. Rev. Appl.*
4 **2017**, *8*, 037001.
5
6 (87) Mayr, C.; Lee, S. Y.; Schmidt, T. D.; Yasuda, T.; Adachi, C.; Brütting, W. Efficiency Enhancement
7 of Organic Light-Emitting Diodes Incorporating a Highly Oriented Thermally Activated Delayed
8 Fluorescence Emitter. *Adv. Funct. Mater.* **2014**, *24*, 5232–5239.
9
10 (88) Lyubimov, I.; Antony, L.; Walters, D. M.; Rodney, D.; Ediger, M. D.; de Pablo, J. J. Orientational
11 Anisotropy in Simulated Vapor-Deposited Molecular Glasses. *J. Chem. Phys.* **2015**, *143*,
12 094502.
13
14 (89) Alessandri, R.; Uusitalo, J. J.; de Vries, A. H.; Havenith, R. W. A.; Marrink, S. J. Bulk
15 Heterojunction Morphologies with Atomistic Resolution from Coarse-Grain Solvent
16 Evaporation Simulations. *J. Am. Chem. Soc.* **2017**, *139*, 3697–3705.
17
18 (90) Moral, M.; Son, W.-J.; Sancho-García, J. C.; Olivier, Y.; Muccioli, L. Cost-Effective Force Field
19 Tailored for Solid-Phase Simulations of OLED Materials. *J. Chem. Theory Comput.* **2015**, *11*,
20 3383–3392.
21
22 (91) Andreussi, O.; Prandi, I. G.; Campetella, M.; Prampolini, G.; Mennucci, B. Classical Force Fields
23 Tailored for QM Applications: Is It Really a Feasible Strategy? *J. Chem. Theory Comput.* **2017**,
24 *13*, 4636–4648.
25
26 (92) Chen, X. K.; Zhang, S. F.; Fan, J. X.; Ren, A. M. Nature of Highly Efficient Thermally Activated
27 Delayed Fluorescence in Organic Light-Emitting Diode Emitters: Nonadiabatic Effect between
28 Excited States. *J. Phys. Chem. C* **2015**, *119*, 9728–9733.
29
30 (93) Wang, L.; Prezhdo, O. V.; Beljonne, D. Mixed Quantum-Classical Dynamics for Charge
31 Transport in Organics. *Phys. Chem. Chem. Phys.* **2015**, *17*, 12395–12406.
32
33 (94) Meyer, H.-D.; Manthe, U.; Cederbaum, L. S. The Multi-Configurational Time-Dependent
34 Hartree Approach. *Chem. Phys. Lett.* **1990**, *165*, 73–78.
35
36 (95) Coropceanu, V.; Sánchez-Carrera, R. S.; Paramonov, P.; Day, G. M.; Brédas, J.-L. Interaction of
37 Charge Carriers with Lattice Vibrations in Organic Molecular Semiconductors: Naphthalene as
38 a Case Study. *J. Phys. Chem. C* **2009**, *113*, 4679–4686.
39
40 (96) Marian, C. M. Mechanism of the Triplet-to-Singlet Upconversion in the Assistant Dopant
41 ACRXTN. *J. Phys. Chem. C* **2016**, *120*, 3715–3721.
42
43 (97) Sun, H.; Hu, Z.; Zhong, C.; Chen, X.; Sun, Z.; Brédas, J.-L. Impact of Dielectric Constant on the
44 Singlet–Triplet Gap in Thermally Activated Delayed Fluorescence Materials. *J. Phys. Chem.*
45 *Lett.* **2017**, *8*, 2393–2398.
46
47 (98) Nakanotani, H.; Higuchi, T.; Furukawa, T.; Masui, K.; Morimoto, K.; Numata, M.; Tanaka, H.;
48 Sagara, Y.; Yasuda, T.; Adachi, C. High-Efficiency Organic Light-Emitting Diodes with
49 Fluorescent Emitters. *Nat. Commun.* **2014**, *5*, 4016.
50
51
52
53
54
55
56
57
58
59
60

- 1
2
3 (99) Dexter, D. L. A Theory of Sensitized Luminescence in Solids. *J. Chem. Phys.* **1953**, *21*, 836–850.
4
5 (100) McConnell, H. M. Intramolecular Charge Transfer in Aromatic Free Radicals. *J. Chem. Phys.*
6 **1961**, *35*, 508–515.
7
8 (101) Beljonne, D.; Curutchet, C.; Scholes, G. D.; Silbey, R. J. Beyond Förster Resonance Energy
9 Transfer in Biological and Nanoscale Systems. *J. Phys. Chem. B* **2009**, *113*, 6583–6599.
10
11 (102) Nakatsuka, S.; Gotoh, H.; Kinoshita, K.; Yasuda, N.; Hatakeyama, T. Divergent Synthesis of
12 Heteroatom-Centered 4,8,12-Triazatriangulenes. *Angew. Chemie Int. Ed.* **2017**, *56*, 5087–
13 5090.
14
15 (103) Matsui, K.; Oda, S.; Yoshiura, K.; Nakajima, K.; Yasuda, N.; Hatakeyama, T. One-Shot Multiple
16 Borylation toward BN-Doped Nanographenes. *J. Am. Chem. Soc.* **2018**, *140*, 1195–1198.
17
18 (104) Hontz, E.; Chang, W.; Congreve, D. N.; Bulović, V.; Baldo, M. A.; Van Voorhis, T. The Role of
19 Electron–Hole Separation in Thermally Activated Delayed Fluorescence in Donor–Acceptor
20 Blends. *J. Phys. Chem. C* **2015**, *119*, 25591–25597.
21
22 (105) Huang, Y.; Westenhoff, S.; Avilov, I.; Sreearunothai, P.; Hodgkiss, J. M.; Deleener, C.; Friend, R.
23 H.; Beljonne, D. Electronic Structures of Interfacial States Formed at Polymeric Semiconductor
24 Heterojunctions. *Nat. Mater.* **2008**, *7*, 483–489.
25
26 (106) Wang, Y.; Sahin-Tiras, K.; Harmon, N. J.; Wohlgenannt, M.; Flatté, M. E. Immense Magnetic
27 Response of Exciplex Light Emission due to Correlated Spin-Charge Dynamics. *Phys. Rev. X*
28 **2016**, *6*, 11011.
29
30 (107) Wykes, M.; Park, S. K.; Bhattacharyya, S.; Varghese, S.; Kwon, J. E.; Whang, D. R.; Cho, I.;
31 Wannemacher, R.; Lüer, L.; Park, S. Y.; et al. Excited State Features and Dynamics in a
32 Distyrylbenzene-Based Mixed Stack Donor–Acceptor Cocrystal with Luminescent Charge
33 Transfer Characteristics. *J. Phys. Chem. Lett.* **2015**, *6*, 3682–3687.
34
35 (108) Wykes, M.; Parambil, R.; Beljonne, D.; Gierschner, J. Vibronic Coupling in Molecular Crystals: A
36 Franck-Condon Herzberg-Teller Model of H-Aggregate Fluorescence Based on Quantum
37 Chemical Cluster Calculations. *J. Chem. Phys.* **2015**, *143*, 114116.
38
39
40
41
42
43
44
45
46
47
48
49
50
51
52
53
54
55
56
57
58
59
60

ACRONYMS

OLED:	Organic Light Emitting Diode
TADF:	Thermally Activated Delayed Fluorescence
IQE:	Internal Quantum Efficiency
T_n :	n-th triplet excited state
S_n :	n-th singlet excited state
(R)ISC:	(Reverse) InterSystem Crossing
D:	Electron donating moiety/unit
A:	Electron accepting moiety/unit
CT:	Charge Transfer
LE:	Local Excitation
DFT:	Density Functional Theory
TD-DFT:	Time-Dependent Density Functional Theory
PCM:	polarizable continuum models [^]
ΔE_{ST}^V :	vertical exchange gap/vertical singlet-triplet energy gap
$\Omega(S_1)$:	Lowest singlet excited state energy
$\Omega(T_1)$:	Lowest triplet excited state energy
CCSDT:	Coupled-Cluster with Single, Double, and (iterative) Triple substitutions
CC3:	Third-Order Approximate Coupled-Cluster
EOM-CCSD:	Equation-Of-Motion Coupled-Cluster with Single and Double substitutions
FCI:	Full Configuration Interactions
CC2:	Second-Order Approximate Coupled-Cluster
ADC(2):	Algebraic Diagrammatic Construction at second-order
ADC(3):	Algebraic Diagrammatic Construction at third-order
ADC(2)-x:	eXtended Algebraic Diagrammatic Construction at second-order
RAS:	Restricted Active Space
CASSCF:	Complete Active Space Self-Consistent-Field
CASPT2:	Complete Active Space Perturbation Theory at second-order
GW+BSE:	Green's functions with Bethe-Salpeter Equation
B3LYP:	Becke three-parameter hybrid Lee-Yang-Parr exchange-correlation functional
6-31G*:	Pople's double- ξ basis set with polarization functions on 2nd row atoms
M06-2X:	Minnesota exchange-correlation functional in its 2006 version
TDA-DFT:	Time-Dependent Density Functional Theory in the Tamm-Dancoff approximation
CIS:	Configuration Interaction with Single substitutions

1		
2		
3	TD-HF:	Time-Dependent Hartree-Fock
4	PBE0:	Perdew-Burke-Ernzerhof one-parameter hybrid exchange-correlation functional
5		
6	D3(BJ):	Dispersion correction (third-generation) with Becke-Johnson attenuation function
7		
8	def2-TZVP:	Alhrichs' triple- ξ valence polarization basis set extended with diffuse function
9		
10	CAM-B3LYP:	Coulomb-attenuating method B3LYP exchange-correlation functional
11	ω B97X:	ω -dependent range-separated Becke'97 exchange-correlation functional
12		
13	HOMO:	Highest-Occupied Molecular Orbital
14		
15	LUMO:	Lowest-Unoccupied Molecular Orbital
16		
17	UKS:	Unrestricted Kohn-Sham
18	ROKS:	Restricted Open-Shell Kohn-Sham
19		
20	sTDA-DFT:	Simplified Tamm-Dancoff Time-Dependent Density Functional Theory
21		
22	sTDA-xTB:	Simplified Tamm-Dancoff Extended Tight-Binding Hamiltonian
23		
24	MP2:	Second order Møller–Plesset perturbation method
25		
26	MRCI:	Multi-Reference Configuration Interaction
27	KS:	Kohn-Sham orbitals
28		
29	NTO:	Natural Transition Orbitals
30		
31	ΔE_{ST} :	Singlet-triplet energy gap
32	ZFS:	Zero-Field Splitting
33		
34	ESR:	Electron Spin Resonance
35		
36	2CzPN:	4,5-di(9h-carbazol-9-yl)phthalonitrile
37		
38	4CzIPN:	1,2,3,5-tetrakis(carbazol-9-yl)-4,6-dicyanobenzene
39	(R)IC:	(Reverse) Internal Conversion
40		
41	MD:	Molecular Dynamics
42		
43	MC:	Monte Carlo
44		
45	QM:	Quantum mechanical
46	S_0 :	Ground state
47		
48	3CT :	Triplet charge transfer state
49		
50	3LE :	Triplet local excitation
51		
52	ϵ :	Dielectric constant
53	PXZ-OXD :	Phenoxazine- 2,5-diphenyl-1,3,4-oxadiazole
54		
55	TXO-TPA:	2- [4- (diphenylamino) phenyl] - 10, 10- dioxide-9H - thioxanthen-9- one
56		
57		
58		
59		
60		

1
2
3
4
5
6
7
8
9
10
11
12
13
14
15
16
17
18
19
20
21
22
23
24
25
26
27
28
29
30
31
32
33
34
35
36
37
38
39
40
41
42
43
44
45
46
47
48
49
50
51
52
53
54
55
56
57
58
59
60

TXO-PhCz: 2- (9- phenyl- 9H-carbazol-3-yl)-10,10- dioxide-9H-thioxanthen-9- one